

Supporting information

Short-bite PSP-type ligands: coordination chemistry and ligand rearrangement reactions

Franziska Flecken,^a Toni Grell^b and Schirin Hanf^{a*}

^a Institute for Inorganic Chemistry, Karlsruhe Institute of Technology, Engesserstr. 15, 76131 Karlsruhe, Germany, schirin.hanf@kit.edu

^b Dipartimento di Chimica, Università degli Studi di Milano, Via Camillo Golgi 19, 20131 Milano, Italy.

1. Experimental section	1
2. NMR and IR spectroscopic analyses	8
3. Single-crystal X-ray crystallography	25
4. Structural parameters	26
5. Literature comparison of ligands.....	28
6. Catalytic tests.....	29
7. Computational details	31
8. References.....	37

1. Experimental section

1.1 Materials, methods and instruments

All experiments were carried out under Ar atmosphere using Schlenk-techniques and an Ar-filled glove box (MBraun). Toluene, tetrahydrofuran (THF), *n*-pentane and *n*-heptane were dried using a solvent purification system (MBraun SPS-800) and degassed prior to use. THF was further distilled over potassium/benzophenone. Acetonitrile (MeCN) and dichloromethane (DCM) were distilled over CaH₂. Deuterated solvents were dried over P₂O₅ (CDCl₃ and CD₂Cl₂) or over CaH₂ (C₆D₆, D₈-toluene and CD₃CN). Before use, deuterated solvents were degassed through three freeze-pump-thaw cycles and stored over molecular sieves (MeCN and CD₃CN over 3 Å, all other over 4 Å).

NMR spectra were recorded on Bruker Avance III or Avance Neo 400 MHz spectrometers at 298 K. Chemical shifts are described in parts per million (ppm) and are referenced to residual solvent signals of the deuterated solvents. For the distinct assignment of the signals, chemical shifts, coupling patterns and 2D experiments (¹H–¹H COSY, ¹H–¹³C HMQC, ¹H–¹³C HMBC) are used. Multiplicities of the NMR signals are abbreviated as s = singlet, d = doublet, t = triplet, dd = doublet of doublets, ddd = doublet of doublets of doublets, dt = doublet of triplets, m = multiplet, br = broad. The NMR data was processed using MestreNova.

Infrared (IR) spectra were conducted using a Bruker Tensor 37 FTIR spectrometer equipped with a room-temperature DLaTGS detector, a diamond ATR (attenuated total reflection) unit, and a nitrogen-flushed measurement chamber in the region of 4000–450 cm⁻¹. Signals were divided into vs = very strong, s = strong, m = medium, w = weak and vw = very weak. Data was processed with the program Origin.

Single crystals were measured on a STOE STADIVARI and on a STOE METAL JET D2 diffractometer. The STOE STADIVARI is equipped with an open Eulerian cradle (4-circle) and a DECTRIS PILATUS pixel detector at 100 K with a microfocus molybdenum source (Mo-Kα, λ = 0.71073 Å) using a graphite monochromator as radiation source. The STOE METAL JET D2 contains a EIGER4M Detector with a sealed X-Ray tube (Mo-Kα, λ = 0.71073 Å) and a graded multilayer mirror monochromator. A liquid-gallium-jet anode is utilized as radiation source. The data reduction was conducted with X-Area version 1.73.1.0 (STOE, 2018)¹ using the semi-empirical absorption correction by X-RED with scaling of the reflection intensities by LANA included in X-Area. Structures were solved by means of dual space methods with SHELXT-2015² and refinement was performed with SHELXL-2018³ using the WinGX⁴ program suite. Full-matrix least-square routines against F² were carried out. Hydrogen atoms were calculated on idealized positions. Pictures were generated with the program DIAMOND⁵. For these thermal ellipsoids are shown with 30% probability and hydrogen atoms as well as co-crystallised solvent molecules are omitted for clarity. CCDC 2375582 (**1**), CCDC 2375583 (**2**),

CCDC 2375585 (**3**), CCDC 2375584 (**4**), and CCDC 2375581 (**5**) contain the supplementary crystallographic data for this paper. These data can and additional information can be obtained free of charge via <https://summary.ccdc.cam.ac.uk/structure-summary-form> (or from the Cambridge Crystallographic Data Centre, 12 Union Road, Cambridge CB2 1EZ, UK; fax: (+44)1223-336-033; or deposit@ccdc.cam.ac.uk).

UV/Vis spectra were recorded using an Ocean FX UV-Vis spectrometer from Ocean Optics. Therefore, solutions with a concentration of $c = 1 \cdot 10^{-4} \text{ mol L}^{-1}$ were prepared. Data was processed with the program Origin.

The elemental analysis of the samples was conducted using a vario EL cube or a vario MICRO cube (Elementar Analysensysteme GmbH).

Catalytic tests were qualitatively and quantitatively evaluated by means of GC-MS using an Agilent 8860 GC and a 5977B MSD whereby *n*-decane was used as internal standard.

1.2 Syntheses

Tetraphenyl diphosphine sulphide ($\text{Ph}_2\text{P(=S)-PPh}_2$, PPS)

PPS was prepared by dissolving diphenyl phosphine sulphide (1 g, 4.582 mmol, 1 eq.) in toluene, adding triethylamine (0.61 g, 0.83 mL, 1.3 eq.) and cooling with an ice bath to 0-5°C. Chlorodiphenylphosphine (1.03 g, 0.84 mL, 4.582 mmol, 1 eq.) diluted in toluene, was added slowly to the solution of diphenyl phosphine sulphide. After stirring overnight, the solution was filtered and the solvent was partially evaporated *in vacuo*. The solution was cooled to -30°C and overnight colourless crystals were grown. The crystals were washed with *n*-pentane and dried *in vacuo* (0.977 g, crystalline yield: 53.0 %).

^1H NMR (298 K, CDCl_3 , 400 MHz), δ [ppm] = 8.14 (m, 4 H), 7.71 (m, 4 H), 6.95 (m, 12 H)

$^{31}\text{P}\{^1\text{H}\}$ NMR (298 K, CD_2Cl_2 , 162 MHz), δ [ppm] = 44.3 (d, P=S, $^2J_{\text{PP}} = 247.3 \text{ Hz}$), -13.8 (d, PPh_2 , $^2J_{\text{PP}} = 247.3 \text{ Hz}$)

[NiBr₂(PSP)] (**1**)

NiBr₂ (100.0 mg, 0.46 mmol, 1 eq.) was heated to reflux with the PPS ($\text{Ph}_2\text{P(=S)-PPh}_2$; 184.2 mg, 0.46 mmol, 1 eq.) ligand in acetonitrile (6 mL) for 5 hours. The reaction mixture was filtered, and the solvent was subsequently removed *in vacuo*. Through redissolving the solid residue in DCM and layering with *n*-heptane, 139.8 mg of compound **1** in 49.2% crystalline yield were obtained.

^1H NMR (298 K, CD_2Cl_2 , 400 MHz), δ [ppm] = 8.11 (m, 8 H, Ph-H-*ortho*), 7.66 (t, 4 H, J_{HH} = 7.6 Hz, Ph-H-*para*); 7.56 (t, 8 H, J_{HH} = 7.6 Hz, Ph-H-*meta*)

$^{31}\text{P}\{^1\text{H}\}$ NMR (298 K, CD_2Cl_2 , 162 MHz), δ [ppm] = -17.5 (s)

^{13}C NMR (298 K, CD_2Cl_2 , 101 MHz), δ [ppm] = 134.0 (br, *o*-Ar-C), 133.1 (s, *p*-Ar-C), 129.5 (br, *m*-Ar-C)

ATR-IR (cm^{-1}): $\tilde{\nu}$ = 1478 (w), 1431(m), 1382(vw), 1330 (vw), 1305 (vw), 1182 (w), 1161 (vw), 1139 (vw), 1088 (m), 1066 (w), 1022 (vw), 995 (w), 970 (vw), 921 (vw), 838 (vw), 754 (w), 740 (s), 710 (w), 694 (m), 682 (vs), 617 (vw), 561 (vs), 534 (w), 507 (vs), 474 (w), 468 (vs), 459 (s), 434 (m)

UV/Vis [dcm, nm ($\text{mol}^{-1}\text{dm}^3\text{cm}^{-1}$): λ_{max} (ϵ) = 510 (2391), 304 (17069), 277 (21175), 255 (24981)

Elemental analysis calculated (%) for $\text{C}_{24}\text{H}_{20}\text{Br}_2\text{NiP}_2\text{S} \cdot 0.5 \text{ DCM}$: C 44.36, H 3.19, S 4.83
found: C 44.36, H 3.26, S 4.88

[NiI₂(PSP)] (2)

NiI₂ (100.0 mg, 0.32 mmol, 1 eq.) and PPS (128.8 mg, 0.32 mmol, 1 eq.) were brought to reflux in acetonitrile (6 mL) for 5 hours. The reaction mixture was filtered. After removing the solvent *in vacuo*, redissolving the resulting solid residue in DCM and layering with *n*-heptane, 105.7 mg of single-crystals were obtained in 46.2 % crystalline yield.

^1H NMR (298 K, CD_2Cl_2 , 400 MHz), δ [ppm] = 8.10 (m, 8 H, *o*-Ph-H), 7.64 (t, 4 H, J_{HH} = 7.5 Hz, *p*-Ph-H); 7.56 (t, 8 H, J_{HH} = 7.5 Hz, *m*-Ph-H)

$^{31}\text{P}\{^1\text{H}\}$ NMR (298 K, CD_2Cl_2 , 162 MHz), δ [ppm] = -14.5 (s)

^{13}C NMR (298 K, CD_2Cl_2 , 101 MHz), δ [ppm] = 134.3 (m, *o*-Ar-C), 132.9 (s, *p*-Ar-C), 129.3 (m, *m*-Ar-C)

ATR-IR (cm^{-1}): $\tilde{\nu}$ = 1478 (w), 1431 (m), 1383 (vw), 1330 (vw), 1303 (vw), 1178 (w), 1161 (vw), 1141 (vw), 1088 (m), 1066 (vw), 1022 (vw), 995 (w), 970 (vw), 923 (vw), 835 (vw), 754 (w), 739 (s), 710 (w), 694 (m), 685 (vs), 615 (vw), 557 (vs), 528 (m), 505 (vs), 474 (w), 464 (s), 453 (s), 434 (m)

UV/Vis (dcm, nm [mol⁻¹dm³cm⁻¹]): λ_{\max} (ϵ) = 564 (2297), 387 (3347), 303 (18242), 250 (24786)

Elemental analysis calculated (%) for C₂₄H₂₀I₂NiP₂S: C 40.32, H 2.82, S 4.48 found: C 40.22, H 3.03, S 4.00

[Ni₂(μ_2 -Ph₂P)(μ_2 -Ph₂PS)(Ph₂PSS)₂] (3)

3 was obtained through the conversion of NiCl₂ (70.0 mg, 0.54 mmol, 1 eq.) and PPS (217.3 mg, 0.54 mmol, 1 eq.) under reflux conditions in acetonitrile (6 mL). After 5 h of reaction, the mixture was filtered and the solvent evaporated *in vacuo*. 17.0 mg of dark-brown crystals suitable for SXRD were obtained by dissolving the solid residue in DCM and layering the solution with *n*-pentane in a crystalline yield of 6 %.

¹H NMR (298 K, CD₂Cl₂, 400 MHz), δ [ppm] = 8.06–7.93 (m, 8 H, *o*-Ph₂PSS⁻), 7.70–7.64 (m, 2 H, *p*-Ph₂PS⁻), 7.64–7.58 (m, 4 H, *o*-Ph₂P⁻), 7.58–7.54 (m, 2 H, *p*-Ph₂P⁻), 7.54–7.48 (m, 4 H, *m*-Ph₂P⁻), 7.48–7.41 (m, 8 H, *o,m*-Ph₂PS⁻), 7.41–7.28 (m, 8 H, *m*-Ph₂PSS⁻), 7.27–7.18 (m, 4 H, *p*-Ph₂PSS⁻)

³¹P{¹H} NMR (298 K, CD₂Cl₂, 162 MHz), δ [ppm] = 92.0 (dt, 1 P_b, Ph₂PS⁻, ²J_{PP} = 49.0 Hz, ³J_{PP} = 3.6 Hz), 72.7 (s, 1 P_d, Ph₂PSS⁻), 72.0 (t, 1 P_a, Ph₂PSS⁻, ³J_{PP} = 3.6 Hz), 60.4 (dd, 1 P_c, Ph₂P⁻, ²J_{PP} = 49.0 Hz, ³J_{PP} = 3.6 Hz); naming scheme: Figure S21

¹³C NMR (298 K, CD₂Cl₂, 101 MHz), δ [ppm] = 135.8 (br), 134.5 (d), 132.8 (d), 131.9 (dd), 130.1 (br), 129.8 (dd), 128.5 (dd), 128.5 (s), 128.0 (d), 127.4 (d)

ATR-IR (cm⁻¹): $\tilde{\nu}$ = 3043 (vw), 1961 (vw), 1877 (vw), 1810 (w), 1774 (w), 1697 (w), 1653 (w), 1616 (vw), 1577 (w), 1561 (w), 1540 (w), 1523 (vw), 1508 (vw), 1475 (m), 1432 (m), 1395 (w), 1328 (w), 1305 (m), 1264 (w), 1179 (m), 1158 (w), 1094 (s), 1067 (m), 1026 (m), 994 (m), 972 (w), 920 (w), 847 (w), 741 (s), 706 (s), 687 (vs), 628 (m), 607 (m), 571 (vs), 520 (m), 488 (s), 475 (s)

Elemental analysis calculated (%) for C₄₈H₄₀Ni₂P₄S₅: C 56.61, H 3.96, S 15.74 found: C 56.24, H 4.03, S 15.97

[Ni₃(μ_2 -Ph₂P)₂(μ_2 -Ph₂PS)₂(Ph₂PS)₂] (4)

[Ni(COD)₂] (50.0 mg, 0.18 mmol, 1 eq.) was reacted with PPS (146.3 mg, 0.36 mmol, 2 eq.) in DCM (6 mL) at room temperature. After stirring overnight, the reaction solution was filtered and layered with *n*-pentane. After 2 days, dark red crystals suitable for single crystal XRD were obtained in 27 % crystalline yield (23.2 mg).

¹H NMR (298 K, CDCl₃, 400 MHz), δ [ppm] = 8.00–7.73 (m, 4 H, *p*-Ph₂PS⁻_{intern}), 7.72–7.57 (m, 4 H, *p*-Ph₂P⁻), 7.56–7.44 (m, 4 H, *p*-Ph₂PS⁻_{terminal}), 7.42–7.27 (m, 8 H, *o*-Ph₂PS⁻_{intern}), 7.28–6.78 (m, 40 H: 8 H *m*-Ph₂PS⁻_{intern}, 8 H *m*-Ph₂P⁻, 8 H *o*-Ph₂P⁻, 8 H *m*-Ph₂PS⁻_{terminal}, 8 H *o*-Ph₂PS⁻_{terminal})

³¹P{¹H} NMR (298 K, CDCl₃, 162 MHz), δ [ppm] = 99.0 (br, 2 P_c, Ph₂PS⁻_{intern}), 40.2 (br, 2 P_b, Ph₂P⁻), 29.6 (br, 1 P_a, Ph₂PS⁻_{terminal}), 22.5 (2 m, 1 P_a, Ph₂PS⁻_{terminal}); naming scheme: Figure S21

¹³C NMR (298 K, CDCl₃, 101 MHz), δ [ppm] = 135.0 (br), 133.9 (br), 133.1–132.3 (br), 128.5 (br), 128.4 (br), 127.1 (br)

Comment on the broadened NMR signals of **4**: The broadening of the NMR signals stems from an increased paramagnetic contribution when the sample is brought into solution. This is due to an equilibrium between the diamagnetic square planar complex **4**, as identified by single crystal XRD, and the paramagnetic tetrahedral analogue. A similar behaviour has been reported before for other Ni(II) complexes, as described in several reviews.⁶⁻⁸ Kläui and co-workers, for example, investigated a phosphine sulphide stabilised dinuclear Ni(II) complex, namely [(C₅H₅)Ni{P(S)R₂}₂Ni(C₅H₅)], which showed a spin-crossover based on geometry changes within the complex.⁹ The authors attributed this behaviour to the strong π -donor character of the sulphur atoms in the phosphine sulfide, which is maximized when the sulphur adopts a nearly planar geometry. For **4**, it can be assumed that mainly the outer nickel atoms are affected by this anomalous behaviour, which are stabilized by terminal Ph₂PS⁻ ligands, since they show the highest deviation from a square-planar coordination (Table S 4).

ATR-IR (cm⁻¹): $\tilde{\nu}$ = 3068 (w), 3049 (w), 1953 (vw), 1882 (vw), 1805 (w), 1772 (vw), 1699 (w), 1650 (w), 1616 (w), 1580 (w), 1558 (w), 1539 (w), 1520 (vw), 1506 (vw), 1475 (m), 1432 (s), 1395 (w), 1323 (w), 1304 (m), 1267 (m), 1243 (m), 1182 (m), 1155 (m), 1128 (m), 1089 (s),

1066 (m), 1026 (m), 997 (m), 968 (w), 918 (w), 844 (w), 736 (s), 687 (vs), 617 (m), 582 (m), 557 (s), 516 (m), 498 (s), 486 (vs), 473 (s)

Elemental analysis calculated (%) for $C_{72}H_{60}Ni_3P_6S_4$: C 61.1, H 4.27, S 9.06 found: C 60.63, H 4.40, S 8.51

[Ni₂(μ₂-Ph₂P)(μ₂-Ph₂PS)(Ph₂PS)(Ph₂PSS)] (5)

[Ni(COD)₂] (50.0 mg, 0.18 mmol, 1 eq.) and KPhPh₂ (93.2 mg, 0.36 mmol, 2 eq.) were dissolved in toluene (6 mL) at room temperature. ClPPH₂ (80.2 mg, 67 μL, 0.36 mmol, 2 eq.) was added and stirred overnight. The reaction mixture was filtered and layered with *n*-pentane affording dark brown crystals in 15 % crystalline yield (13.3 mg).

¹H NMR (298 K, CD₂Cl₂, 400 MHz), δ [ppm] = 8.08–7.97 (m, 4 H, *o*-Ph₂PSS⁻), 7.68–7.57 (m, 4 H, *o*-Ph₂PS^{-intern}), 7.57–7.35 (m, 18 H: 4 H, *m*-Ph₂PSS⁻, 2 H, *p*-Ph₂PSS⁻, 4 H, *m*-Ph₂PS^{-intern}, 2 H, *p*-Ph₂PSS⁻, 2 H, *p*-Ph₂P⁻, 4 H, *m*-Ph₂PS^{-terminal}) 7.30–7.18 (m, 4 H, *o*-Ph₂PS^{-terminal}), 7.18–7.09 (m, 4 H, *m*-Ph₂P⁻), 7.03–6.96 (m, 2 H, *p*-Ph₂PS^{-terminal}), 6.96–6.85 (m, 4 H, *o*-Ph₂P⁻)

³¹P{¹H} NMR (298 K, CD₂Cl₂, 162 MHz), δ [ppm] = 90.1 (ddd, 1 P_b, Ph₂PS^{-intern}, ²J_{PP} = 42.9 Hz, ³J_{PP} = 6.7 Hz, ³J_{PP} = 3.3 Hz), 73.0 (t, 1 P_a, Ph₂PSS⁻, ³J_{PP} = 3.3 Hz), 56.3 (ddd, 1 P_c, Ph₂P⁻, ²J_{PP} = 42.9 Hz, ²J_{PP} = 31.0 Hz, ³J_{PP} = 3.3 Hz), 31.0 (dd, 1 P_d, Ph₂PS^{-terminal}, ²J_{PP} = 31.0 Hz, ³J_{PP} = 6.7 Hz); naming scheme: Figure S21

¹³C NMR (298 K, CD₂Cl₂, 101 MHz), δ [ppm] = 134.3 (d), 133.4–133.0 (m), 132.2 (br), 131.2 (br), 130.2 (d), 128.8 (t), 128.7 (br), 128.4 (br), 127.7 (br), 127.6 (br)

ATR-IR (cm⁻¹): $\tilde{\nu}$ = 3068 (vw), 3049 (vw), 1801 (vw), 1770 (vw), 1699 (vw), 1681 (vw), 1648 (vw), 1581 (w), 1558 (vw), 1539 (vw), 1523 (vw), 1506 (vw), 1475 (w), 1433 (m), 1389 (vw), 1327 (vw), 1306 (w), 1273 (vw), 1182 (w), 1157 (w), 1093 (m), 1068 (w), 1026 (w), 997 (w), 970 (vw), 919 (vw), 847 (vw), 741 (s), 689 (vs), 635 (vw), 619 (vw), 577 (m), 559 (s), 517 (m), 488 (vs)

Elemental analysis calculated (%) for $C_{48}H_{40}Ni_2P_4S_4 \cdot 0.7$ toluene: C 60.46, H 4.37, S 12.2 found: C 60.45, H 4.81, S 11.76

1.3 Catalytic tests

All catalytic tests have been conducted under Argon atmosphere in Young-NMR tubes at room temperature. All catalytic tests were carried out with **1**, **2** and simultaneously with the reference catalyst [NiBr₂(dppe)]. The substrates (aryl halide, 0.1 mmol) and Grignard reagent (1.0 eq., 0.1 mmol), catalyst (5.0 mol%), and the internal standard *n*-decane (20 μL) were dissolved in the solvent (0.5 mL; THF, benzene or toluene). For C(*sp*²)-C(*sp*³) couplings, 10 mol% of the catalysts were used. During the addition of the reagents, the reaction mixture was cooled down to 0–5°C and the mixture was allowed to slowly reach room temperature overnight. After completion of the reaction time (20 h if not noted otherwise), the reaction mixture was filtered and analysed using GC-MS (100 μL sample in 1 mL EtOH).

2. NMR and IR spectroscopic analyses

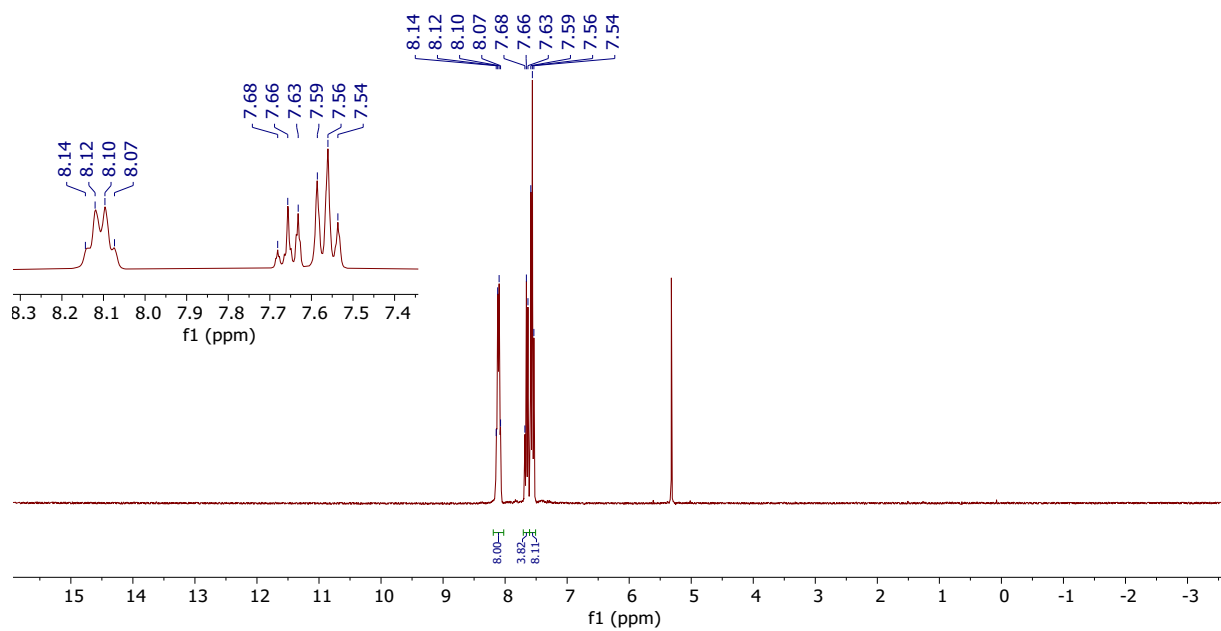


Figure S 1. ^1H NMR (298 K, CD_2Cl_2 , 400 MHz) spectrum of $[\text{NiBr}_2(\text{PSP})]$ (1).

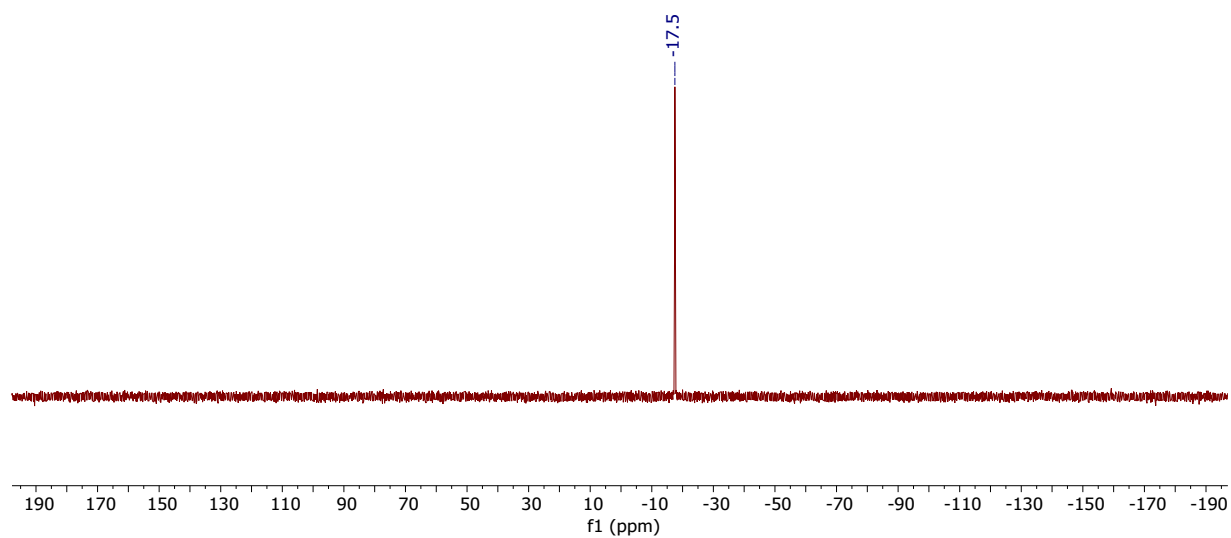


Figure S 2. $^{31}\text{P}\{^1\text{H}\}$ NMR (298 K, CD_2Cl_2 , 162 MHz) spectrum of $[\text{NiBr}_2(\text{PSP})]$ (1).

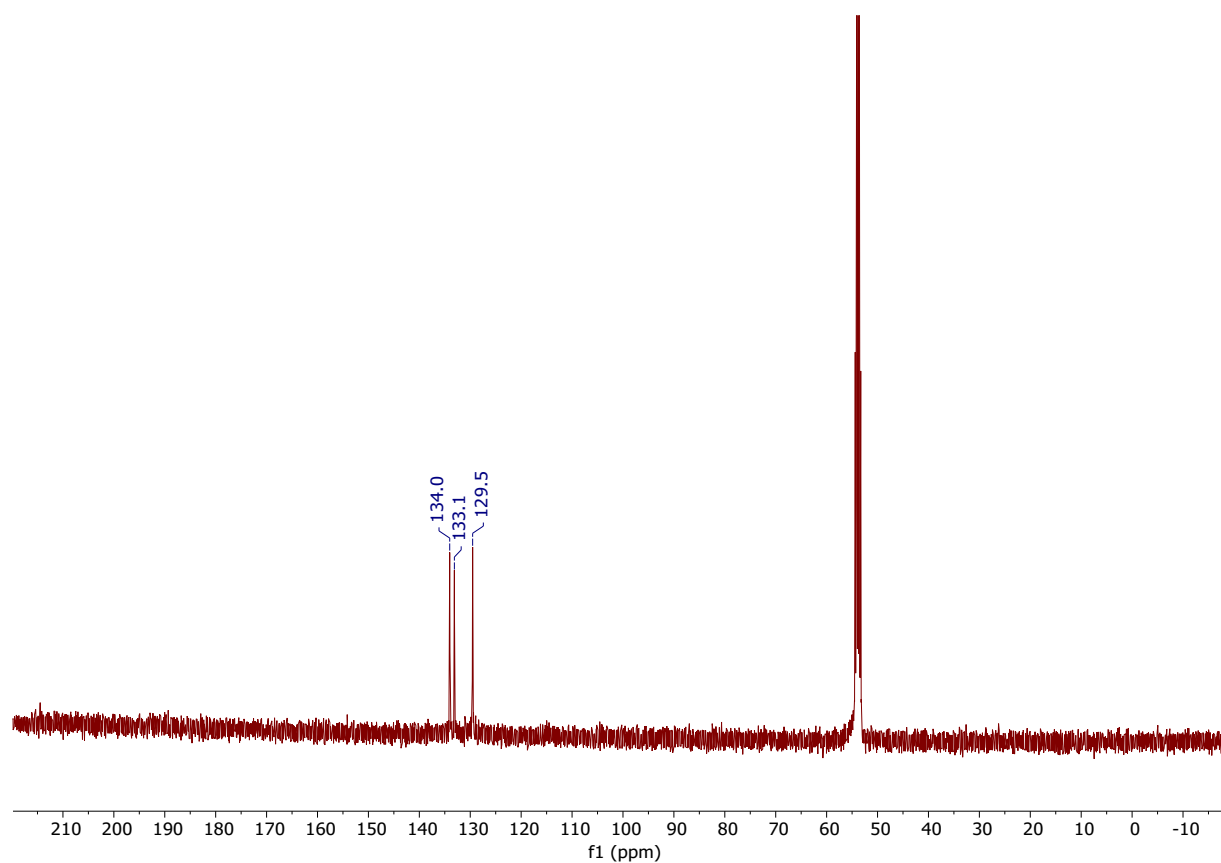


Figure S 3. ^{13}C NMR (298 K, CD_2Cl_2 , 101 MHz) spectrum of $[\text{NiBr}_2(\text{PSP})]$ (1).

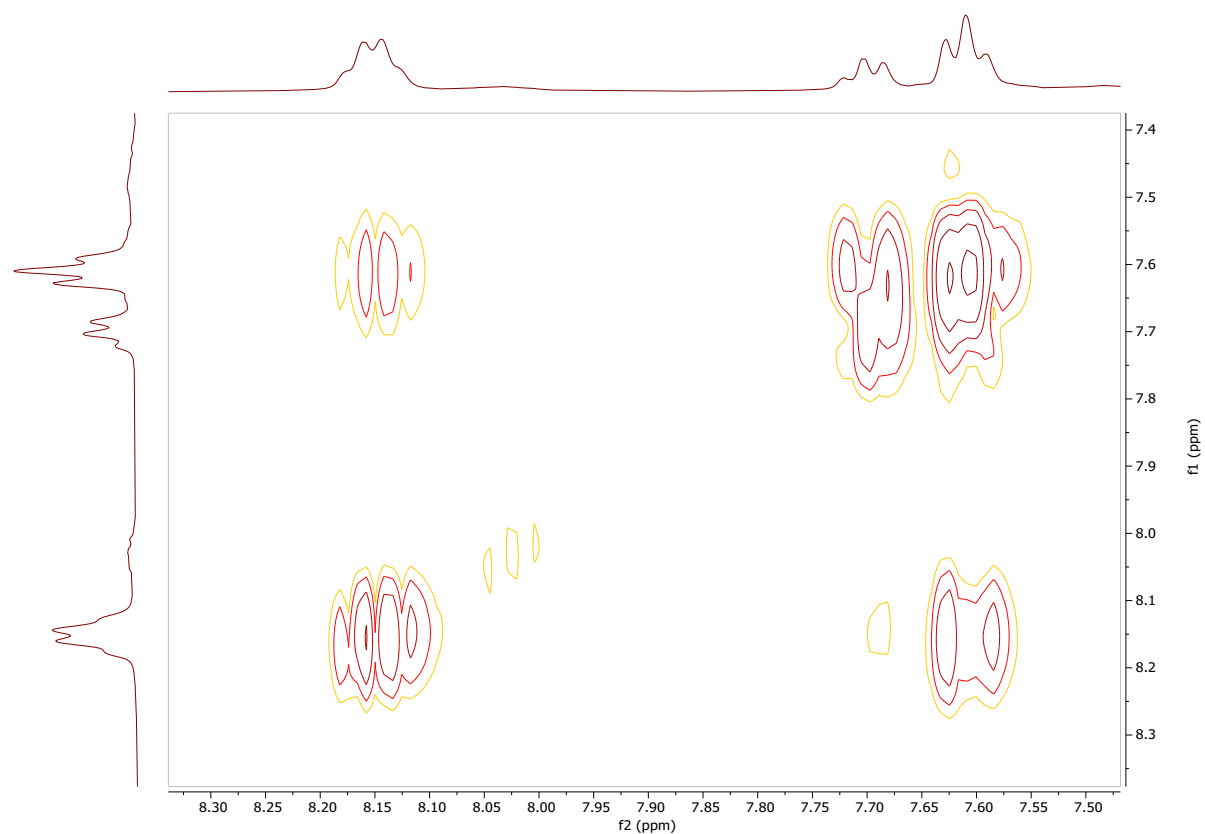


Figure S 4: ^1H - ^1H COSY NMR (298 K, CD_2Cl_2 , 400 MHz) spectrum of $[\text{NiBr}_2(\text{PSP})]$ (**1**).

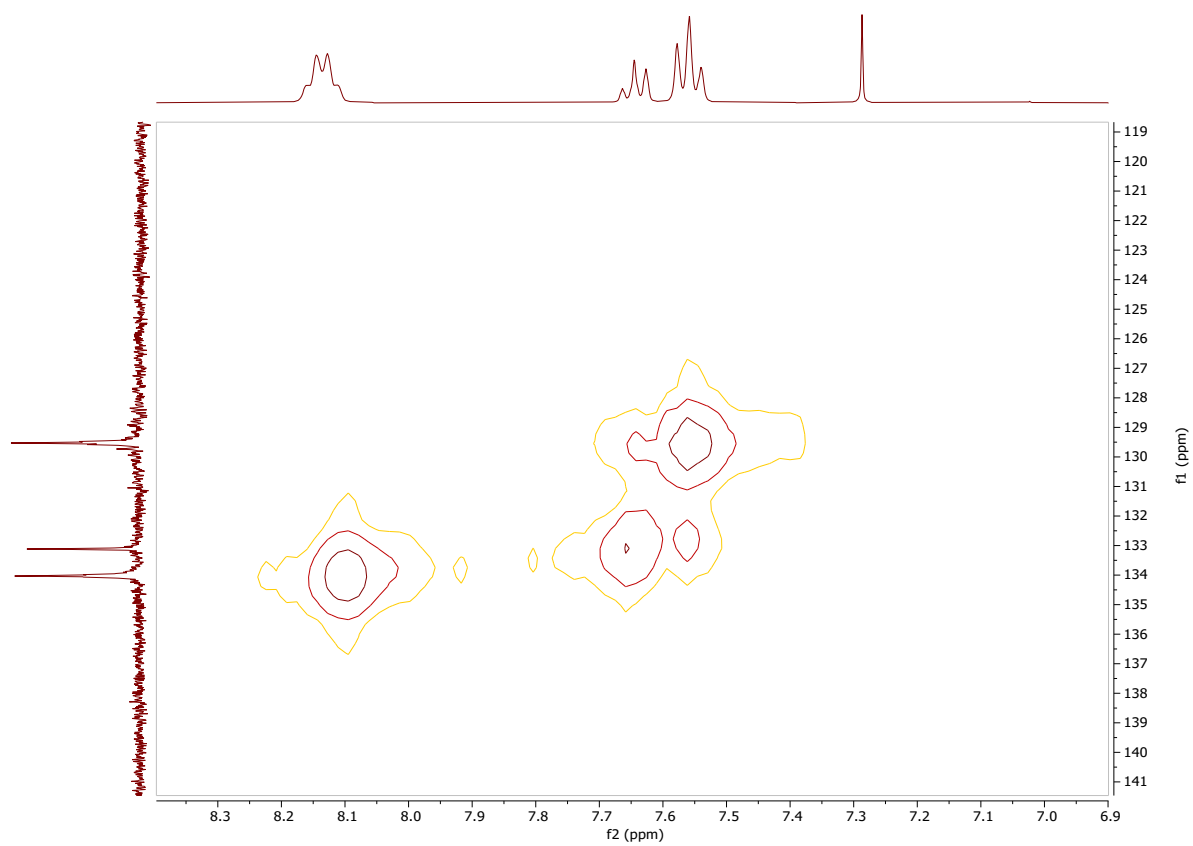


Figure S 5. ^1H - ^{13}C HMQC NMR (298 K, CD_2Cl_2 , 400 MHz, 101 MHz) spectrum of $[\text{NiBr}_2(\text{PSP})]$ (1).

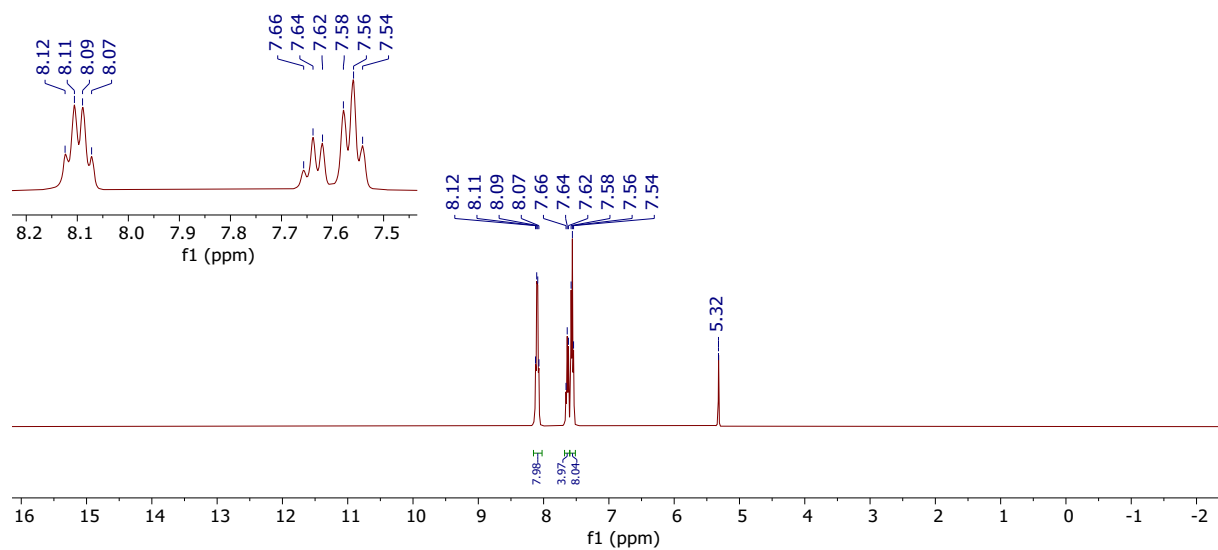


Figure S 6. ¹H NMR (298 K, CD₂Cl₂, 400 MHz) spectrum of [NiI₂(PSP)] (2).

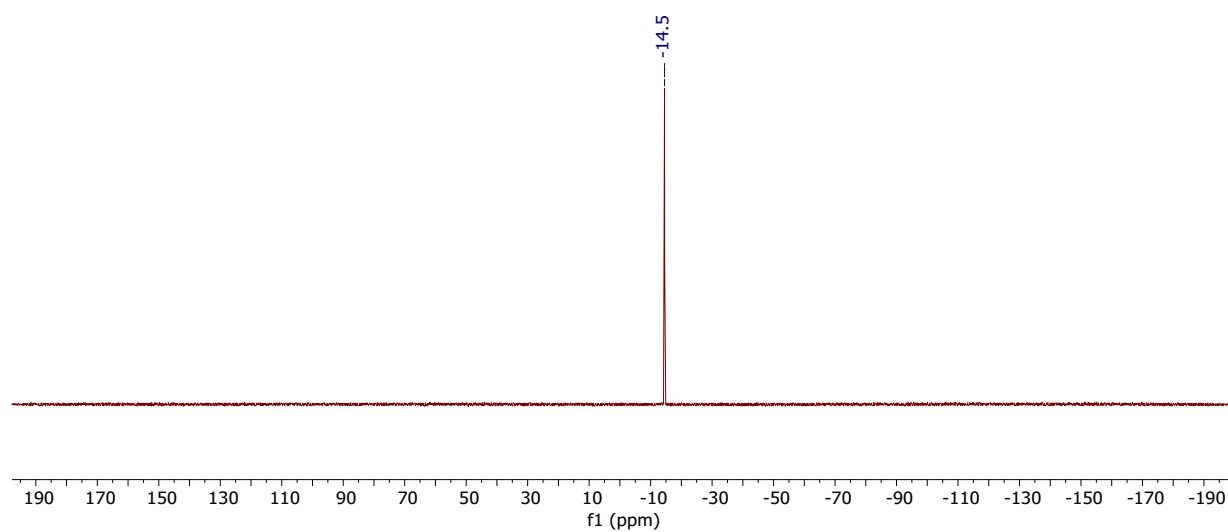


Figure S 7. ³¹P{¹H} NMR (298 K, CD₂Cl₂, 162 MHz) spectrum of [NiI₂(PSP)] (2).

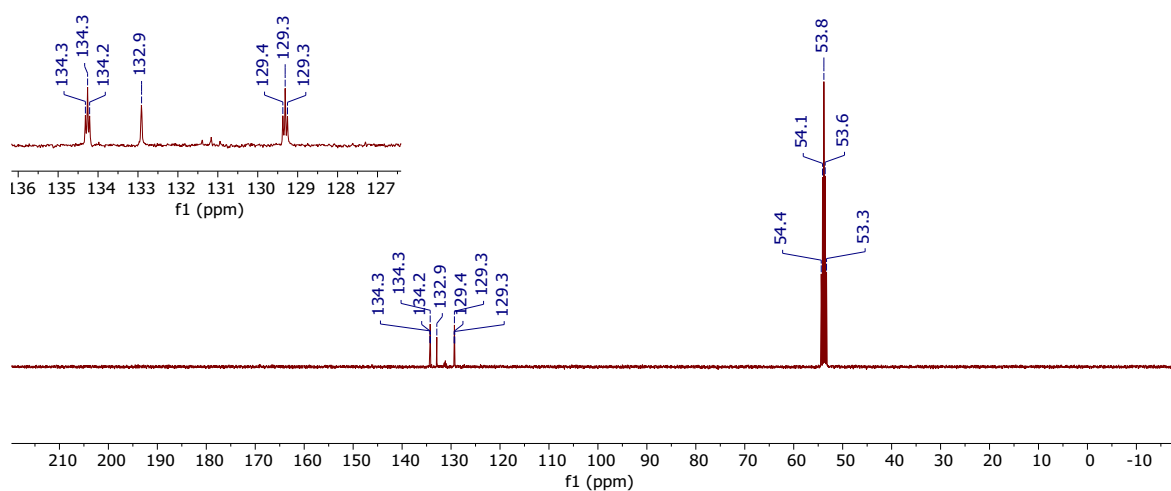


Figure S 8. ¹³C NMR (298 K, CD₂Cl₂, 101 MHz) spectrum of [NiI₂(PSP)] (2).

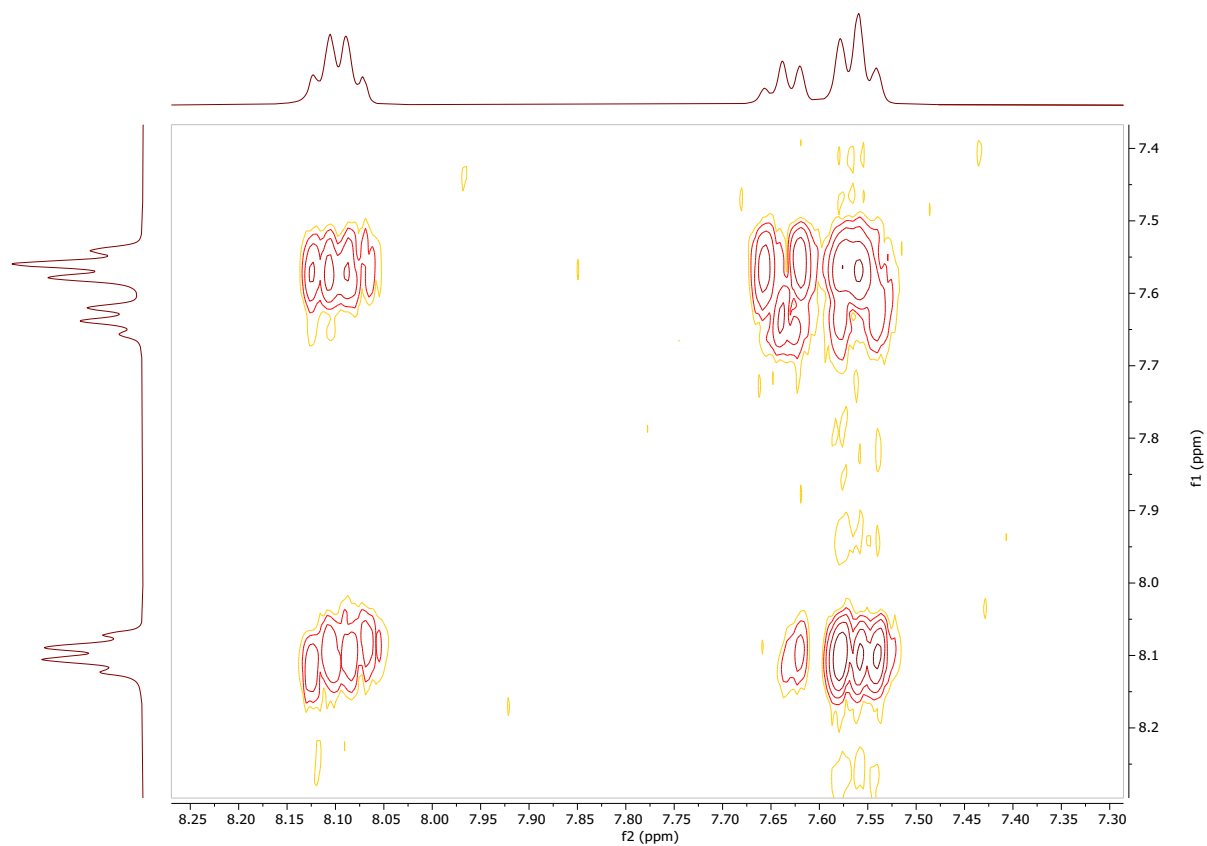


Figure S 9. ¹H-¹H COSY NMR (298 K, CD₂Cl₂, 400 MHz) spectrum of [NiI₂(PSP)] (2).

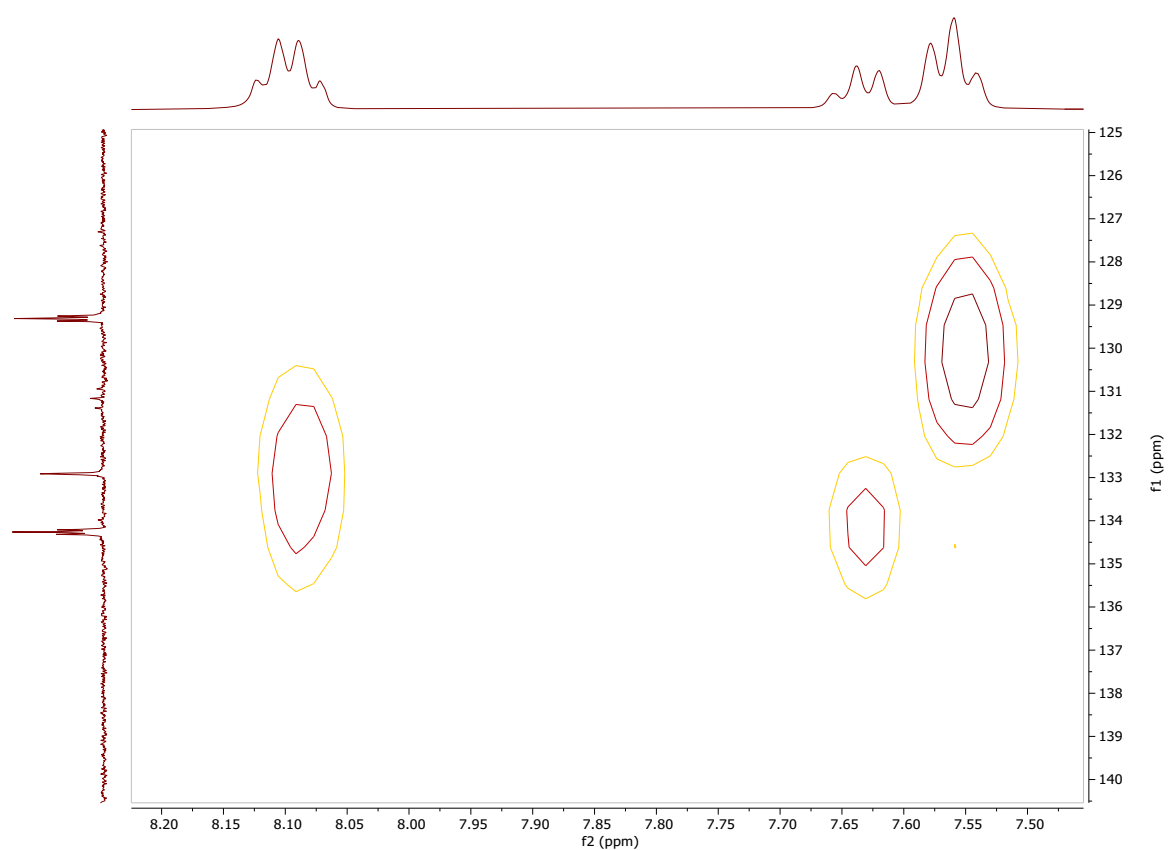


Figure S 10. HMQC NMR (298 K, CD_2Cl_2 , 400 MHz, 101 MHz) spectrum of $[\text{NiI}_2(\text{PSP})]$ (2).

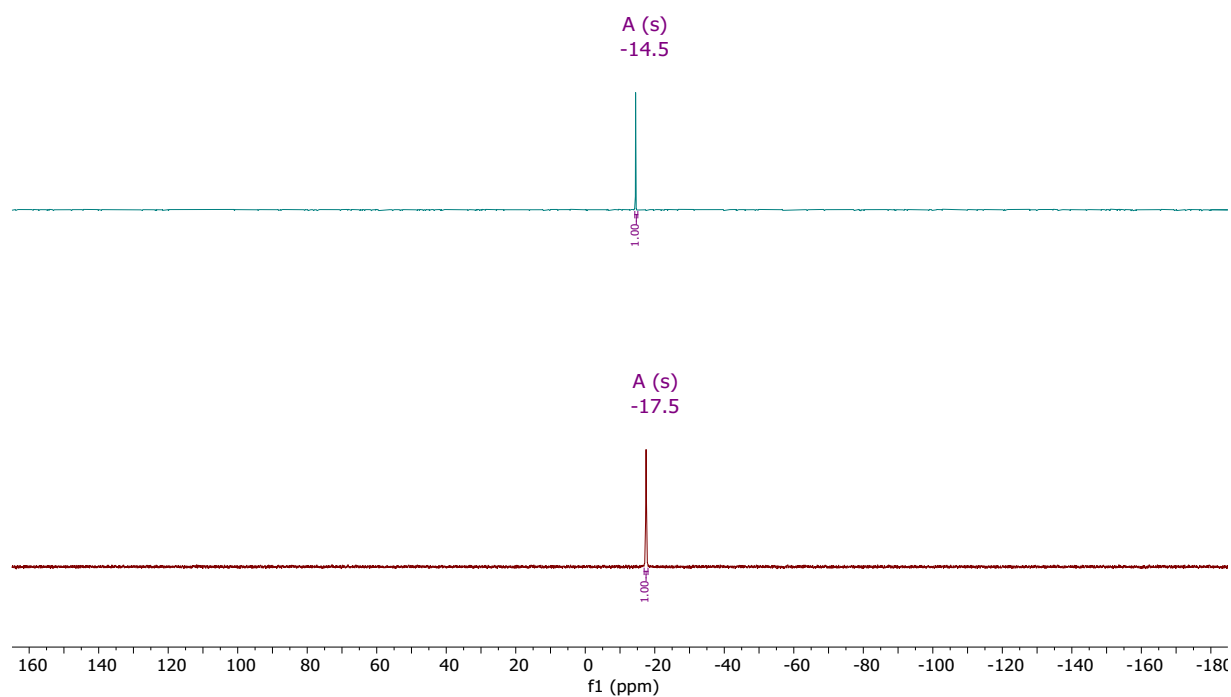


Figure S 11. $^{31}\text{P}\{^1\text{H}\}$ NMR (298 K, CD_2Cl_2 , 162 MHz) spectra of compounds **1** and **2** in solution after UV light (365 nm) radiation overnight. No formation of multinuclear compounds, such as **3-5**, or any other change of **1** and **2** can be observed.

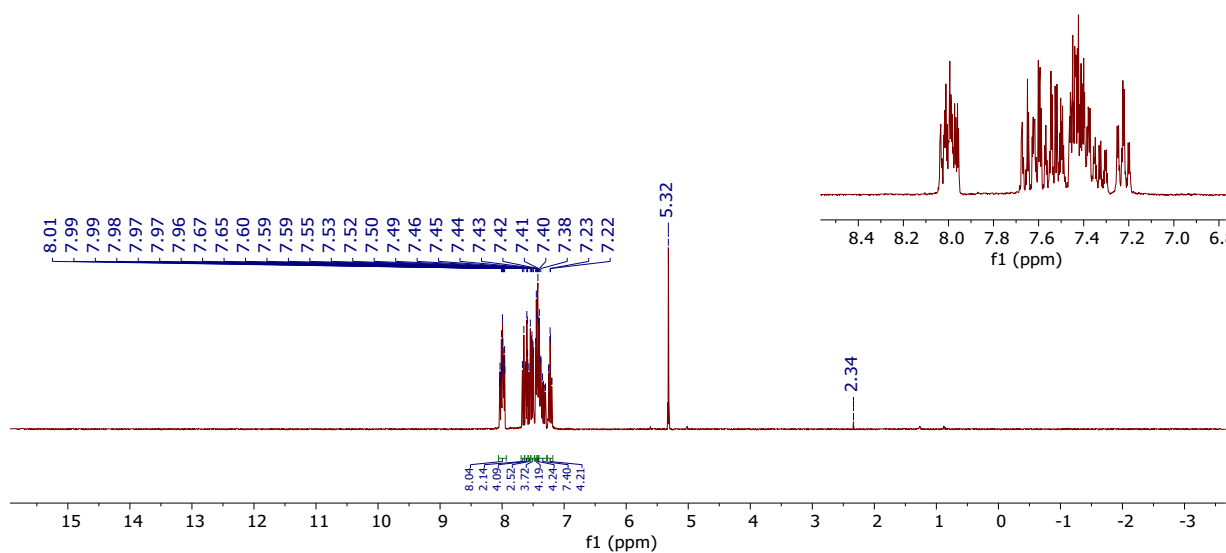


Figure S 12. ¹H NMR (298 K, CD₂Cl₂, 400 MHz) spectrum of 3.

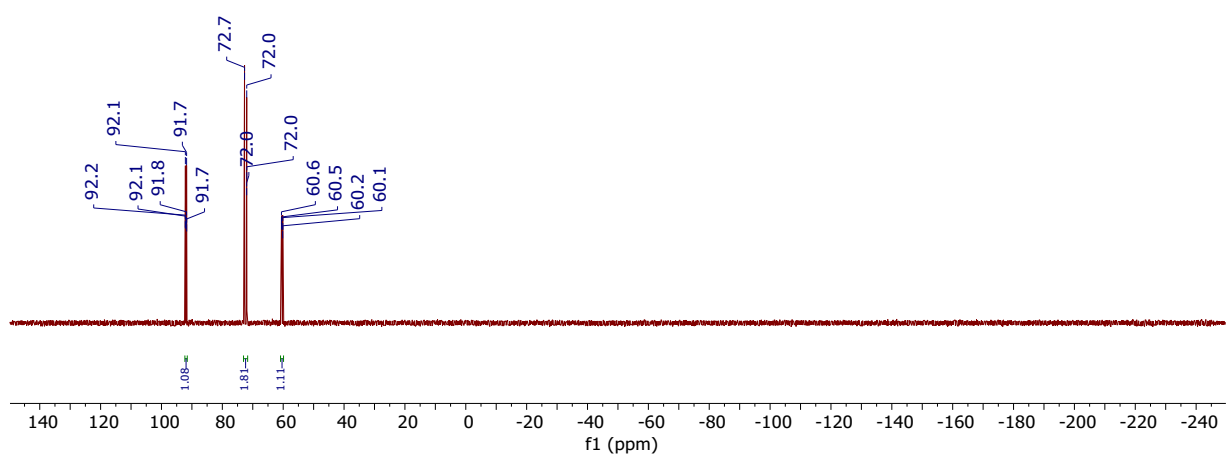


Figure S 13. ³¹P{¹H} NMR (298 K, CD₂Cl₂, 162 MHz) spectrum of 3.

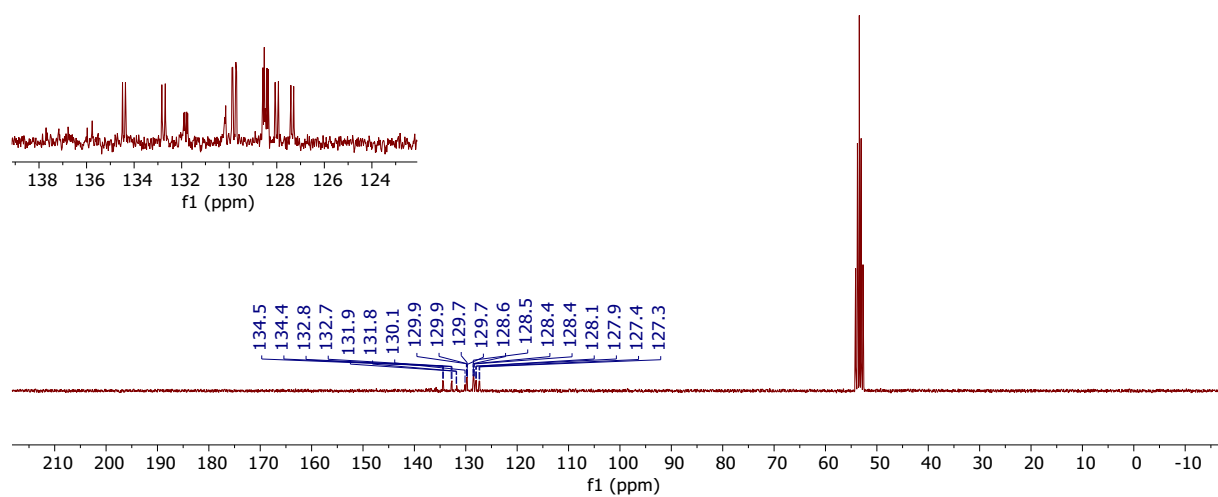


Figure S 14. ^{13}C NMR (298 K, CD_2Cl_2 , 101 MHz) spectrum of 3.

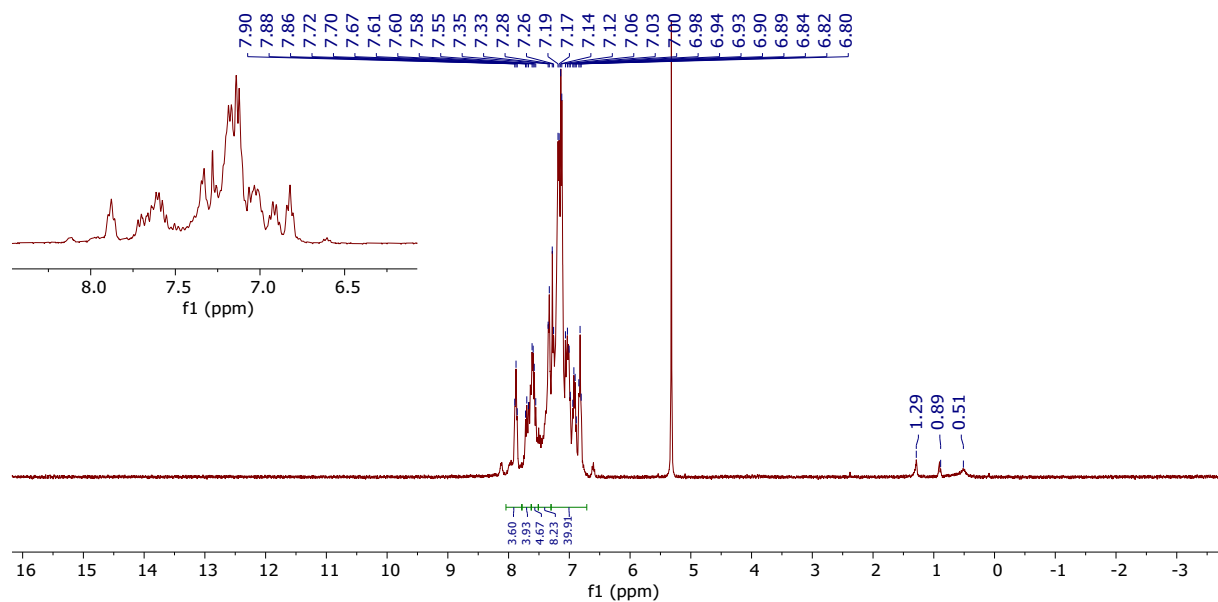


Figure S 15. ¹H NMR (298 K, CDCl₃, 400 MHz) spectrum of 4. Signals at 1.29 and 0.89 are caused by residual *n*-pentane.

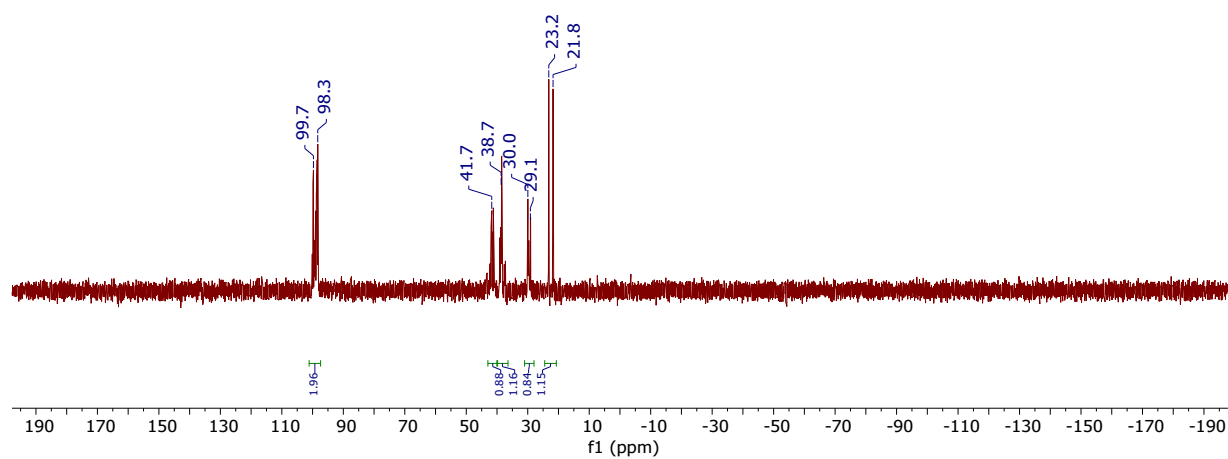


Figure S 16. $^{31}\text{P}\{^1\text{H}\}$ NMR (298 K, CDCl_3 , 162 MHz) spectrum of 4.

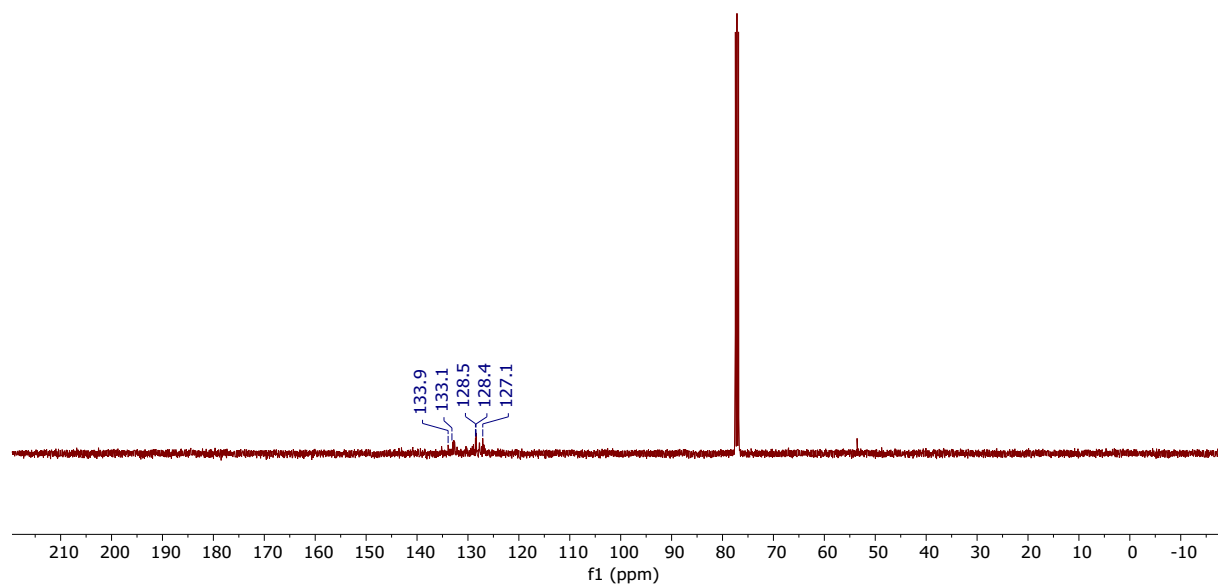


Figure S 17. ^{13}C NMR (298 K, CDCl_3 , 101 MHz) spectrum of 4.

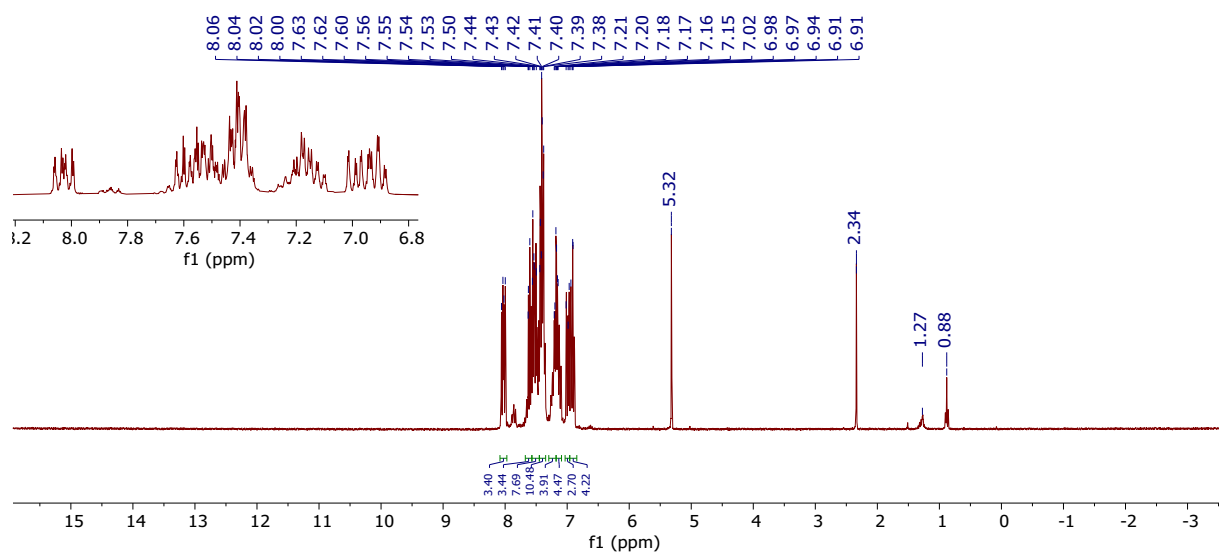


Figure S 18. ^1H NMR (298 K, CD_2Cl_2 , 400 MHz) spectrum of 5. Remaining solvent residues of toluene and pentane are visible, as found in the solid-state structure of 5.

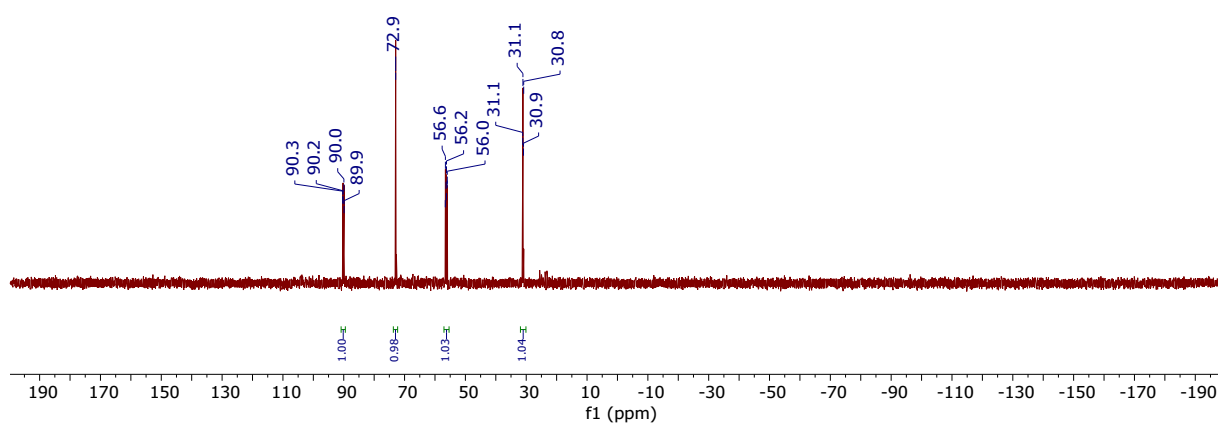


Figure S 19. $^{31}\text{P}\{^1\text{H}\}$ NMR (298 K, CD_2Cl_2 , 162 MHz) spectrum of 5.

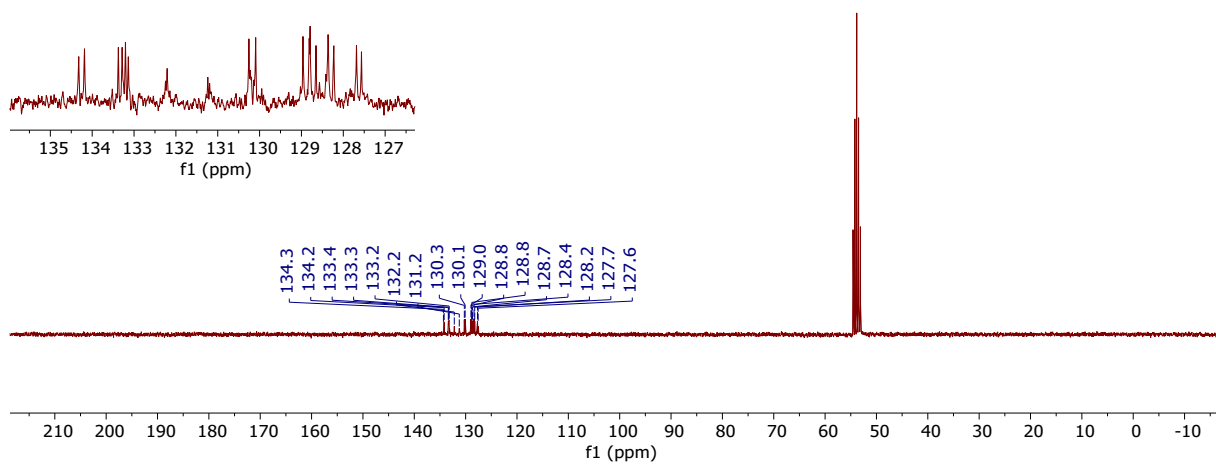


Figure S 20. ^{13}C NMR (298 K, CD_2Cl_2 , 101 MHz) spectrum of 5.

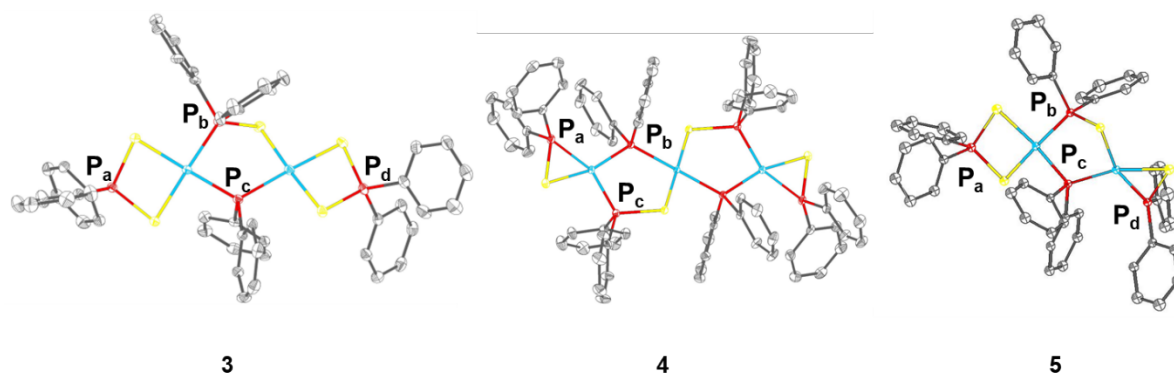


Figure S 21. Naming scheme for the assignment of the signals in compounds 3, 4, 5 in $^{31}\text{P}\{^1\text{H}\}$ NMR spectra.

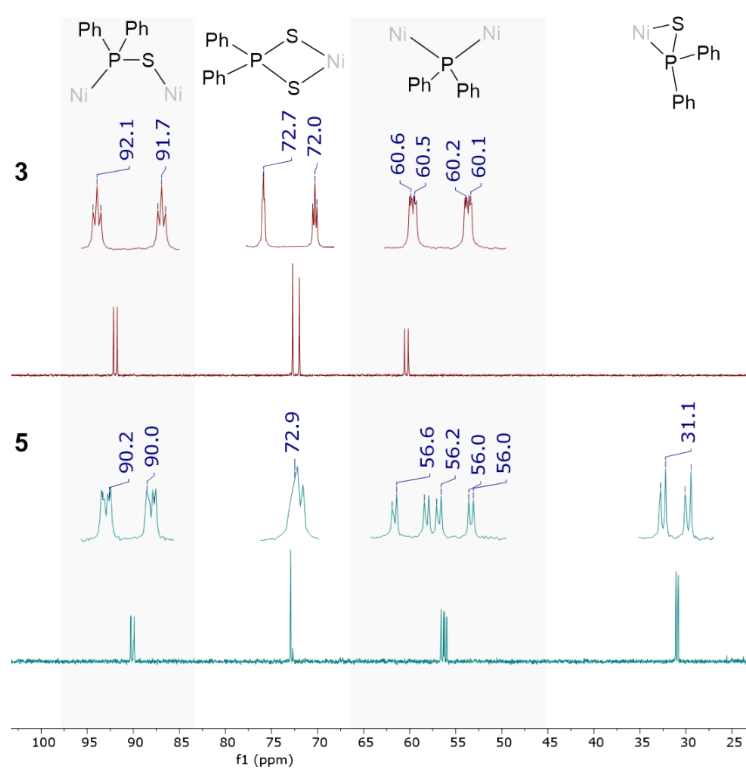


Figure S 22. $^{31}\text{P}\{^1\text{H}\}$ NMR (298 K, CD_2Cl_2 , 162 MHz) spectra of 3 and 5 and assignment of the signals.

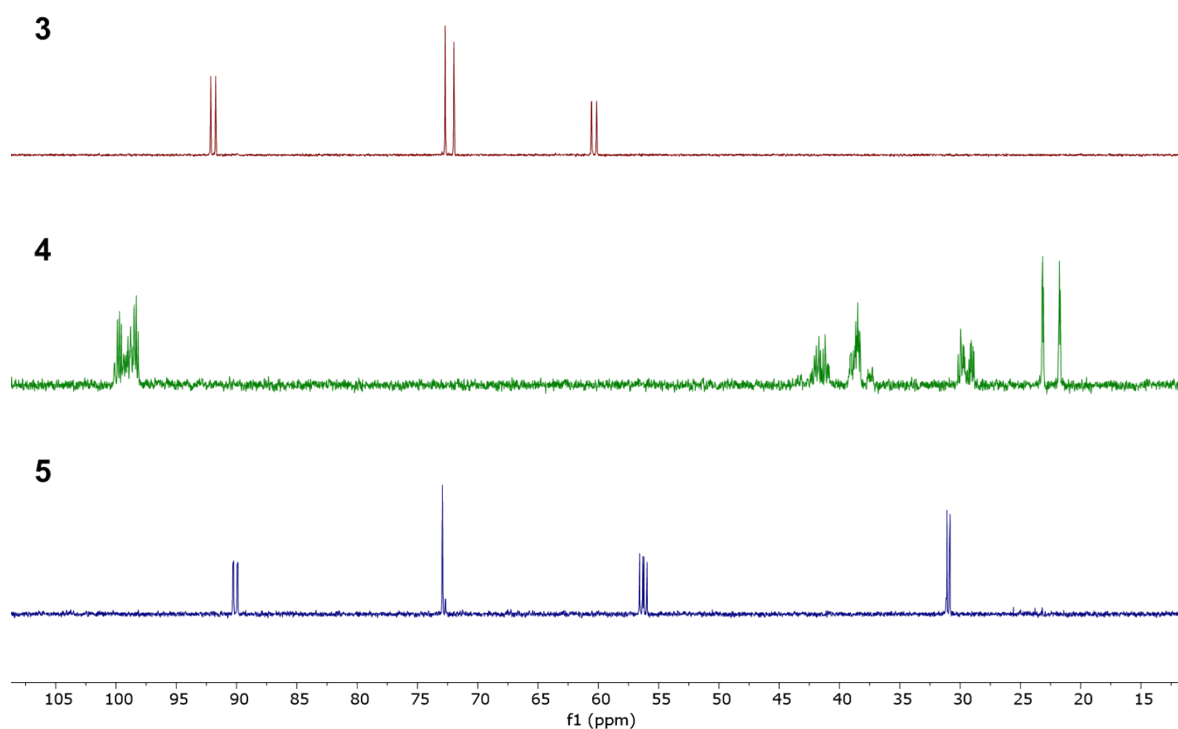


Figure S 23. Comparison of the $^{31}\text{P}\{^1\text{H}\}$ NMR (298 K, CD_2Cl_2 (3, 5) or CDCl_3 (4), 162 MHz) spectra for the assignment of the phosphorus-based signals.

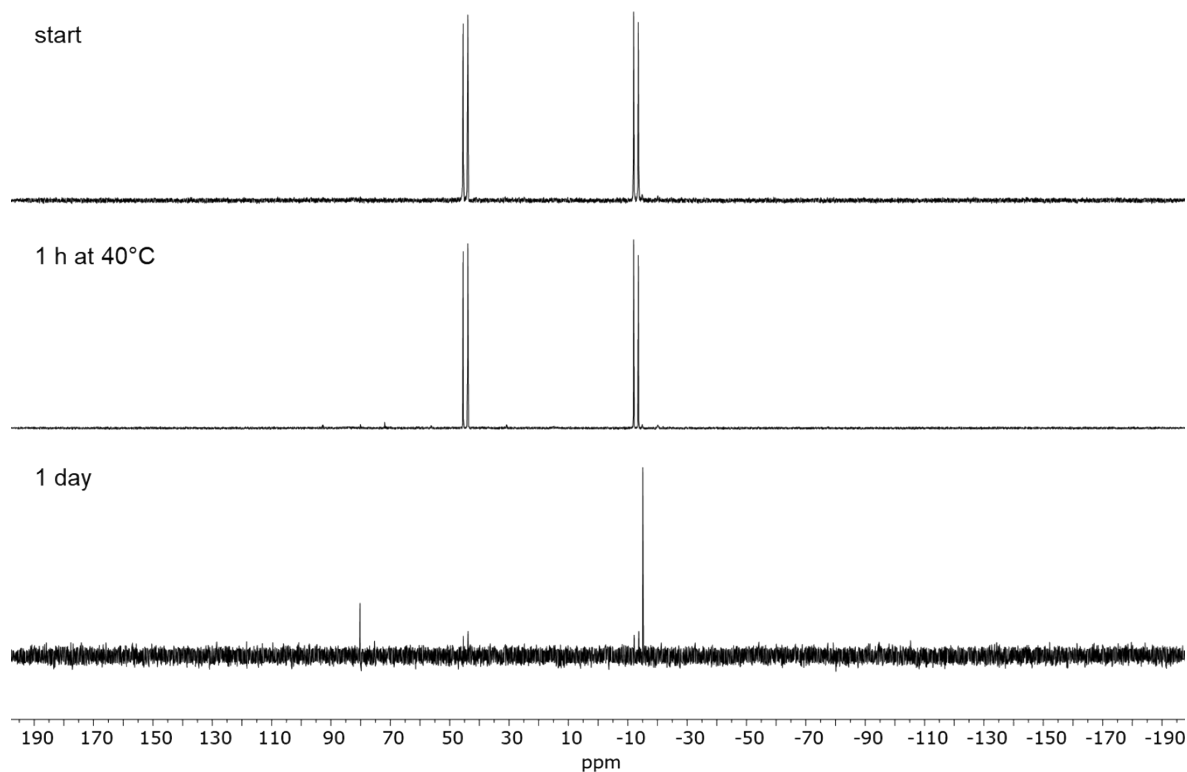


Figure S 24. $^{31}\text{P}\{^1\text{H}\}$ NMR (298 K, CD_2Cl_2 , 162 MHz) of the NMR scale reaction of $[\text{Ni}(\text{COD})_2]$ and PPS. At the start of the reaction and after heating to 40°C for 1 h, the unreacted PPS ligand is the only species that can be observed. After 1 day, the PPS ligand is consumed and $\text{Ph}_2\text{P}-\text{PPh}_2$ is mainly detected, which stems from ligand rearrangement reactions yielding Ph_2PSS^- , Ph_2PS^- and Ph_2P^- . In addition, trace amounts of an

unidentified species at 80.2 ppm can be observed. However, the formation of intermediate species of the synthesis of **4** cannot be tracked by NMR spectroscopy due to their paramagnetic character.

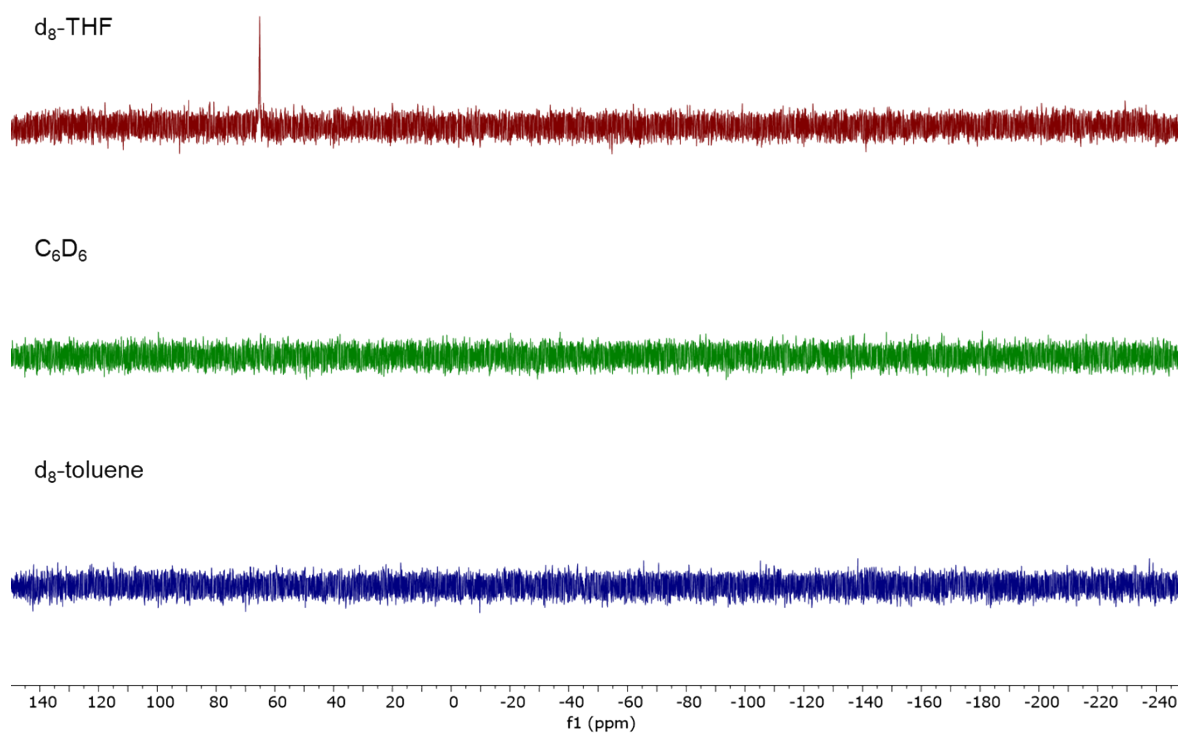


Figure S 25. Investigation of the solution behaviour of the reference catalyst $[\text{NiBr}_2(\text{dppe})]$ in $\text{d}_8\text{-thf}$, C_6D_6 and $\text{d}_8\text{-toluene}$ via $^{31}\text{P}\{^1\text{H}\}$ NMR spectroscopy (298 K, 162 MHz). The compound is only sufficiently soluble in $\text{d}_8\text{-thf}$ for the detection of NMR signals. No ligand dissociation can be identified.

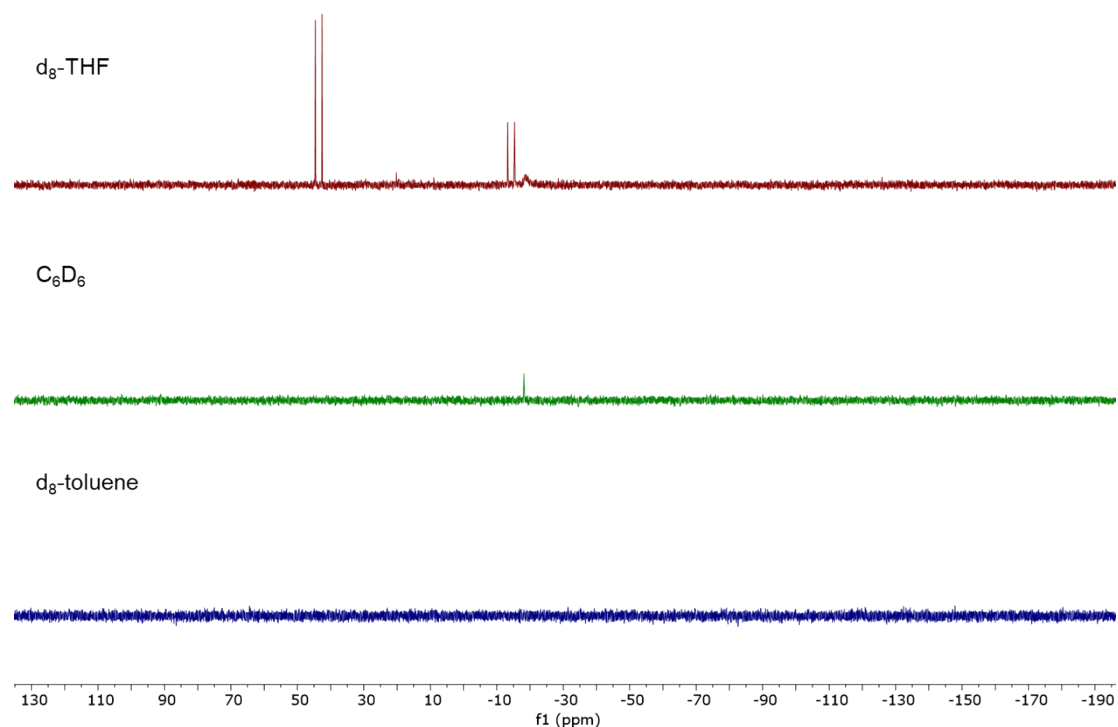


Figure S 26. Investigation of the solution behaviour of 1 in $\text{d}_8\text{-thf}$, C_6D_6 and $\text{d}_8\text{-toluene}$ via $^{31}\text{P}\{^1\text{H}\}$ NMR spectroscopy (298 K, 162 MHz). In $\text{d}_8\text{-thf}$, PPS ($\delta = 43.9$ ppm, d, $\text{P}=\text{S}$, $^1J_{\text{PP}} = 247.3$ Hz; -14.0 ppm, d, PPh_2 , $^1J_{\text{PP}} = 247.3$ Hz) is liberated pointing towards the ligand substitution by THF, in C_6D_6 only the signal of 1 is visible and in $\text{d}_8\text{-toluene}$ no sufficient amount of compound can be dissolved.

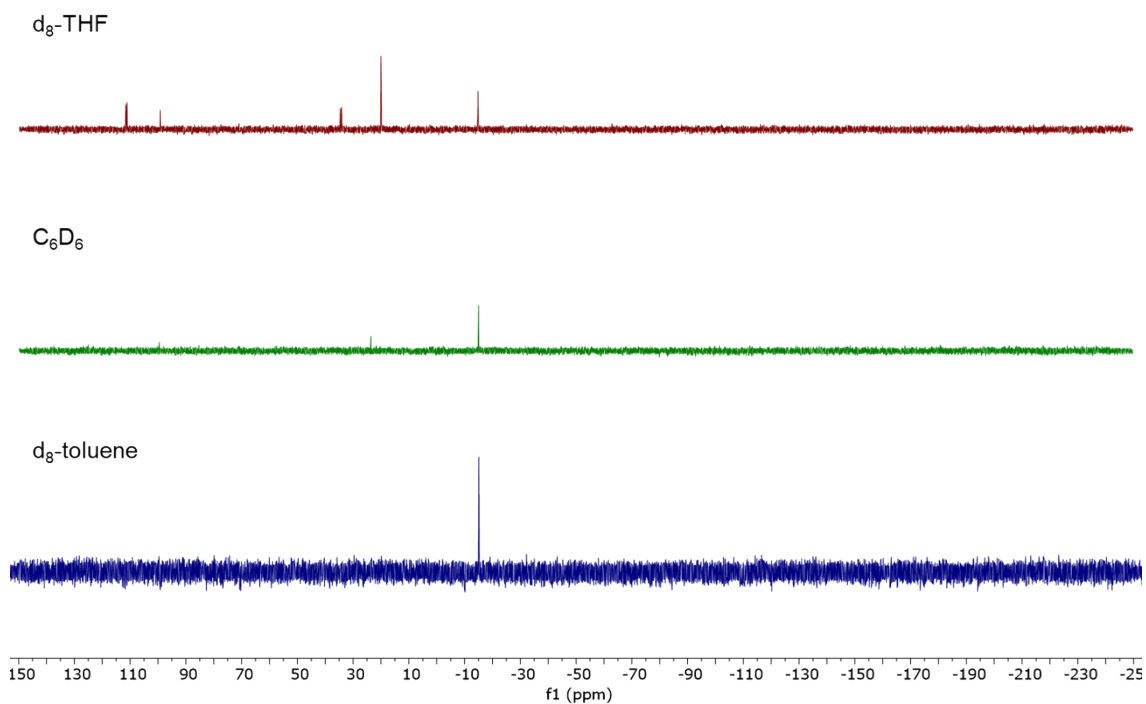


Figure S 27. Investigation of the solution behaviour of 2 in $\text{d}_8\text{-thf}$, C_6D_6 and $\text{d}_8\text{-toluene}$ via $^{31}\text{P}\{^1\text{H}\}$ NMR spectroscopy (298 K, 162 MHz). In $\text{d}_8\text{-thf}$, unlike with 1, no PPS is liberated. Instead, new compounds are formed, which reveal different environments of phosphorus (111.6 ppm (d, 51.5 Hz), 99.5 ppm (s), 34.7 ppm (d, 51.5 Hz), 20.3 ppm (s), -14.5 ppm (s, 2) through association of thf. Hereby it is likely that the coordination

of thf causes a shift of the PSP tautomeric form to the PPS tautomeric form. In C_6D_6 mainly the signal of 2 is visible and slight amounts of similar compounds as in d_8 -thf. In d_8 -toluene 2 can be dissolved.

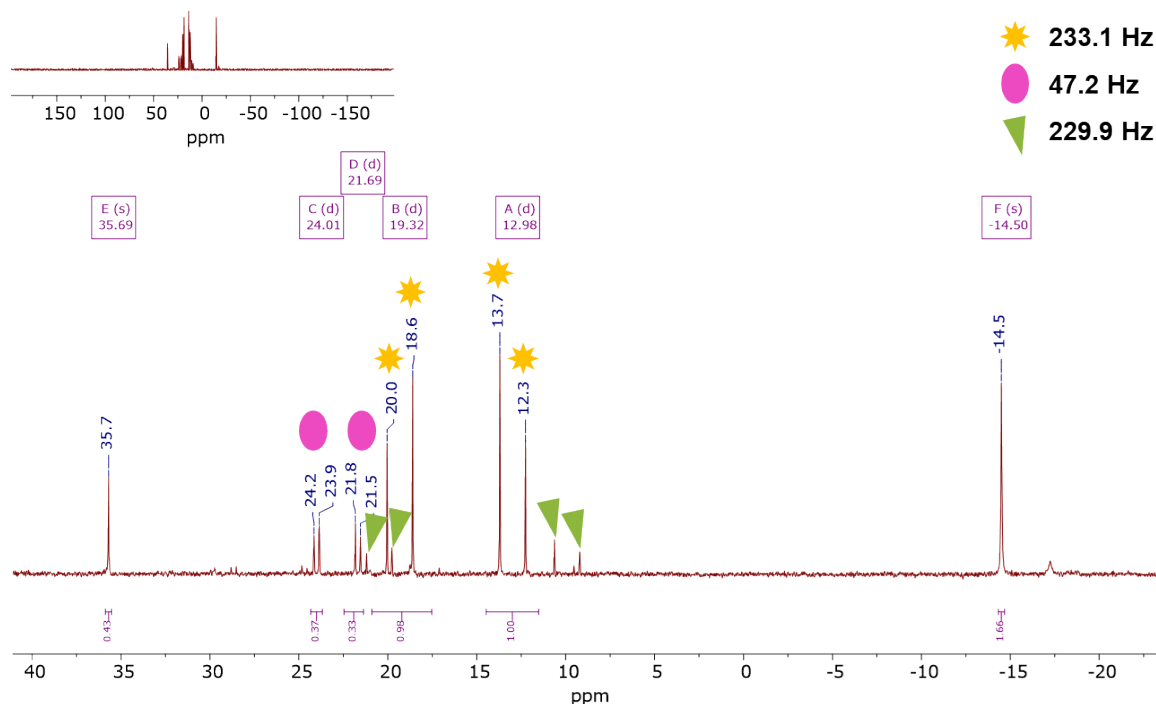


Figure S 28. Conversion of 2 with 2 eq. of MesMgBr in CDCl₃ tracked using ³¹P{¹H} NMR spectroscopy (298 K, 162 MHz). Besides the consumption of 2 (−14.5 ppm), new compounds are formed, which result in several doublets of doublets. The signals are highly likely stemming from [Ni(Mes)(PSP)] and complexes containing the PPS tautomer of the ligand coordinated to Ni(II) or Ni(0). An analogue behaviour is observed with 1 eq. and 2 eq. of MesMgBr in CDCl₃ and toluene, whereby an increased consumption of 2 is achieved with a larger quantity of MesMgBr and better solubility in CDCl₃ compared to toluene. It should be noted that no liberated PPS ligand can be observed.

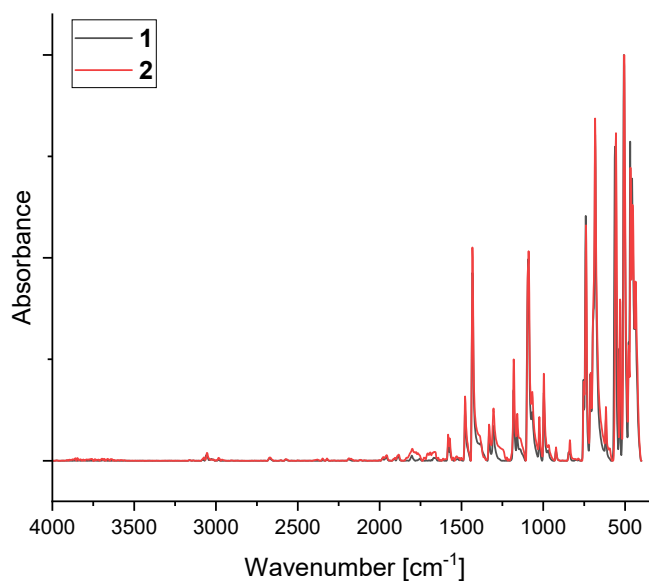


Figure S 29. Normalized IR spectra of 1 and 2, recorded at 298 K in nitrogen.

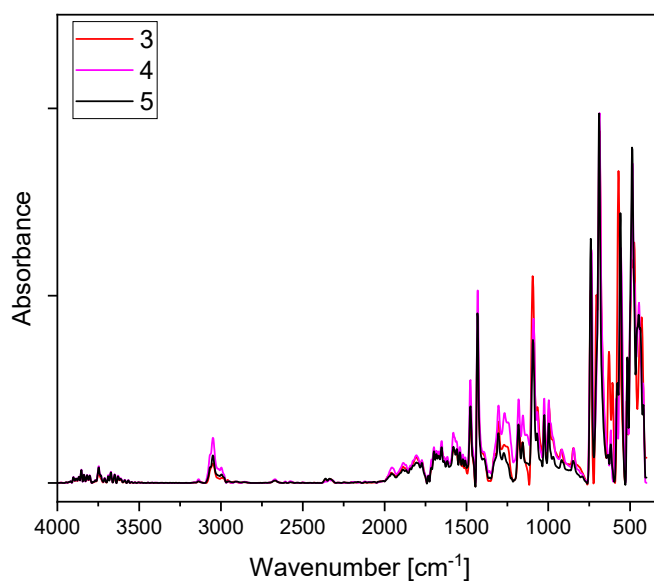


Figure S 30. Normalized IR spectra of 3, 4 and 5, recorded at 298 K in nitrogen.

3. Single-crystal X-ray crystallography

Table S 1: Crystallographic parameters of the complexes 1–5.

	1	2	3	4 · DCM	5 · 1 toluene · 1 n-pentane
CCDC No.	2375582	2375583	2375585	2375584	2375581
Formulae	$C_{24}H_{20}SP_2NiBr$ r_2	$C_{24}H_{20}SP_2Ni$ I_2	$C_{48}H_{40}S_5P_4$ Ni_2	$C_{74}H_{46}S_4P_6Ni_3$ Cl_4	$C_{108}H_{100}S_8P_8$ Ni_4
Formula mass	620.93	714.91	1018.40	1585.24	2136.96
Crystal system	monoclinic	Monoclinic	triclinic	monoclinic	triclinic
Space group	$P2_1/n$	$I2$	$P\bar{1}$	$P2_1/n$	$P\bar{1}$
T [K]	180	150	180	180	100
a [Å]	8.6617(4)	11.983(10)	13.7840(4)	12.1053(5)	13.2596(3)
b [Å]	14.1619(5)	7.826(4)	16.4338(5)	13.2856(4)	20.2572(6)
c [Å]	19.4168(11)	14.014(12)	21.9103(7)	22.4508(9)	20.9388(6)
α [°]	90	90	93.043(2)	90	115.888(2)
β [°]	92.730(4)	108.88(4)	96.228(2)	96.619(3)	99.709(2)
γ [°]	90	90	110.795(2)	90	90.394(2)
V [Å ³]	2379.08(19)	1243.5(16)	4590.0(2)	3586.6(2)	4966.7(2)
Z	4	2	4	2	2
Radiation type	Ga-K α	Ga-K α	Ga-K α	Ga-K α	Mo-K α
μ [mm ⁻¹]	8.692	19.034	7.003	6.946	1.092
No. of reflections	15738	6318	59741	40865	73285

measured					
No. of independent reflections	5261	1900	18781	8653	24081
R_{int}	0.0219	0.0540	0.0397	0.0266	0.0932
Final R_1 values ($I > 2\sigma(I)$)	0.0276	0.0387	0.0374	0.0319	0.0455
Final $wR(F^2)$ values ($I > 2\sigma(I)$)	0.0714	0.1099	0.0728	0.0720	0.1178
Final R_1 values (all data)	0.0318	0.0387	0.0797	0.0439	0.0659
Final $wR(F^2)$ values (all data)	0.0732	0.1099	0.0815	0.0768	0.1294
Goodness of fit on F^2	1.044	1.066	0.890	1.026	1.023

4. Structural parameters

Table S 2. Selected bond lengths [Å], angles [°] and structural parameters of 1 and 2 in the solid-state.

	[NiBr ₂ (PSP)] (1)	[NiI ₂ (PSP)] (2)
P–S	2.1146(7)–2.1183(7)	2.117(3)
P–Ni	2.1347(6)–2.1425(6)	2.137(3)
Ni–X	2.3271(4)–2.3370(4)	2.5251(7)
P–C	1.799(2)–1.812(2)	1.814(6)–1.816(7)
X–Ni–X	97.234(13)	100.57(8)
X–Ni–P	91.613(19)–171.07(2)	89.93(7)–167.36(6)
Ni–P–S	99.43(3)–99.80(3)	98.93(10)
P–S–P	80.81(3)	81.51(15)
P–Ni–P	79.80(2)	80.62(13)
Distance Ni–best plane ^a	0.008	0.000
τ'_4 ^b	0.13	0.18

^a The best plane is defined by the two P-atoms of the PSP ligand and two halides; distance to this plane is given in Å; ^b Structural index parameter¹⁰: $\tau'_4 [-] = ((\beta - \alpha)/(360 - \theta)) + ((180 - \beta)/(180 - \theta))$, β, α : largest valence angles $\beta > \alpha$, θ : tetrahedral angle $\cos^{-1}(-1/3) \sim 109.47^\circ$; $\tau'_4 \sim 0$ for square planar and $\tau'_4 \sim 1$ for tetrahedral coordination

Table S 3. Selected bond lengths [Å] in the different ligands (Ph₂PS⁻, Ph₂PSS⁻ and Ph₂P⁻) of the multinuclear Ni complexes 3, 4 and 5.

Compound	Ligand	P–S	P–Ni	S–Ni
3	Ph ₂ PS ₂ ⁻	1.9949(11)– 2.0176(10)	2.8200(8)– 2.8385(8) ^a	2.2311(9)– 2.2826(8)
5	Ph ₂ PS ₂ ⁻	2.0084(10)– 2.0086(10)	2.8208(7) ^a	2.2428(7)– 2.2664(8)
3	Ph ₂ PS ⁻ (intern.)	2.0357(10)– 2.0394(10)	2.1448(9)– 2.1467(8)	2.1784(9)– 2.1900(9)
4	Ph ₂ PS ⁻ (term.)	2.0246(7)	2.1477(5)	2.2102(5)
4	Ph ₂ PS ⁻ (intern.)	2.0616(6)	2.1353(5)	2.1739(4)
5	Ph ₂ PS ⁻ (term.)	2.0064(10)	2.0962(7)	2.2498(7)
5	Ph ₂ PS ⁻ (intern.)	2.0421(9)	2.1642(7)	2.2078(7)
3	Ph ₂ P ⁻	-	2.1999(8)– 2.2045(8)	-
4	Ph ₂ P ⁻	-	2.1844(5); 2.2711(4)	-
5	Ph ₂ P ⁻	-	2.1665(7); 2.1915(7)	-

^a Atom–Atom distance, no direct bond

Table S 4. Classification of the coordination environments in 3-5 based on the distance of the Ni(II) atoms to the best plane [Å] and on the structural index parameter τ'_4 [-]

	3	4	5
Distance Ni–best plane ^a	0.003–0.079	0.000–0.099 ^c	0.001–0.056 ^d
τ'_4 ^b	0.03–0.10	0.000–0.24 ^c	0.13–0.27 ^d

^a The best plane is defined by the four coordinating P and S atoms of the ligands; ^b Structural index parameter¹⁰: τ'_4 [-] = $((\beta-\alpha)/(360-\theta)) + ((180-\beta)/(180-\theta))$, β, α : largest valence angles $\beta > \alpha$, θ : tetrahedral angle $\cos^{-1}(-1/3) \sim 109.47^\circ$; $\tau'_4 \sim 0$ for square planar and $\tau'_4 \sim 1$ for tetrahedral coordination ^c the central Ni atom shows an ideal square planar geometry whereas the outer two Ni atoms show larger deviations induced by the coordination of the terminal Ph₂PS⁻ ligand ^d the terminal Ph₂PS⁻ ligand again results in a decreased ideal square planar geometry while for the Ni atom coordinated by the terminal Ph₂PSS⁻ ligand smaller deviations from the ideal square planar geometry can be obtained

5. Literature comparison of ligands

Table S 5. PSP-containing literature reported transition metal chelate complexes with selected bond lengths (Å) and angles (°).

Compound	P–S	P–M	P–S–P	P–M–P	Reference
	2.131(3)	2.489(2)	86.9(1)	72.02(7)	11
	2.126(6)– 2.145(6)	2.278(4)– 2.288(4)	82.1(2)	75.8(2)	12
	2.126(4)– 2.136(4)	2.302(2)– 2.315(2)	82.19(9)	74.71(6)	12
	2.123(4)– 2.135(4)	2.299(2)– 2.306(2)	82.46(9)	74.90(6)	12

Table S 6. Literature reported transition metal complexes with Ph₂PS[–], Ph₂P[–] and Ph₂PSS[–] ligands and selected bond lengths (Å).

Compound	Ligand	P–S	P–Ni	S–Ni	Reference
	Ph ₂ PS [–]	2.0600(7)– 2.0648(7)	2.1440(6)– 2.1555(6)	2.1979(5)– 2.1986(6)	13,14
	Ph ₂ PSS [–]	2.006(8)– 2.022(8)	-	2.234(5)– 2.242(6)	15
	Ph ₂ PSS [–]	1.993(6)– 2.013(6)	-	2.482(4)– 2.523(3)	16
	Ph ₂ P [–]	-	2.153–2.156	-	17
	Ph ₂ P [–]	-	2.173(1)– 2.184(1)	-	18

6. Catalytic tests

Table S 7. Catalytic test results using **1**, **2** or [NiBr₂(dppe)] (ref) as catalysts in the coupling reaction of aryl halides and Grignard reagents. Reaction conditions: aryl halide (1 eq.) and Grignard reagent (1 eq.) are reacted in the named solvents for 20 h at room temperature. The conversions of aryl halides were determined by GC-MS using *n*-decane as internal standard.

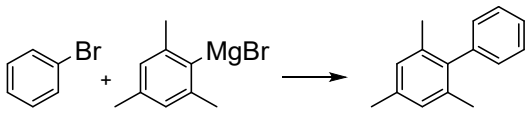

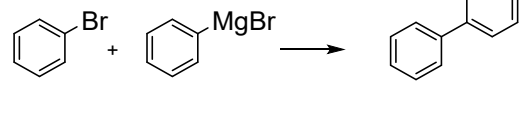
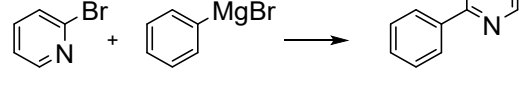
		Conversion [%]			Selectivity [%]		
		THF	C ₆ D ₆	Tol.	THF	C ₆ D ₆	Tol.
	1	45	26	63	100	100	100
	2	48	14	52	100	100	100
	ref	74	0	14	100	-	100
	1	39	69	75	50	90	91
	2	28	75	82	63	95	86
	ref	20	29	53	61	100	100
	1	58	40	50	100	100	94
	2	45	46	49	100	100	85
	ref	72	73	62	100	100	100
	1	84	46	79	55	78	72
	2	76	20	77	63	84	79
	ref	84	42	86	95	94	92

Table S 8. Catalytic results using **1**, **2** or the reference catalyst ("ref") [NiBr₂(dppe)] for C(sp²)-C(sp²) couplings with sterically demanding arylbromides. Reactions were carried out with 10 mol% catalyst at room temperature for 20 h in toluene.

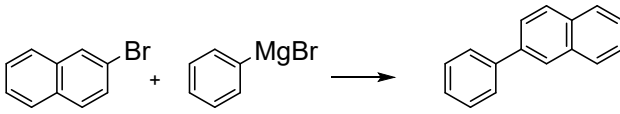
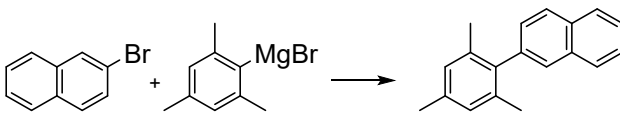
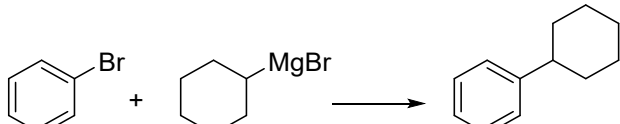
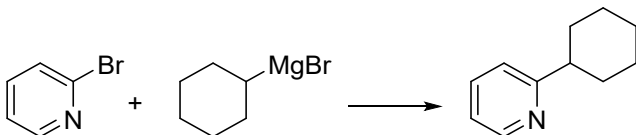
		Conversion [%]	Selectivity [%]
	1	91	100
	2	80	100
	ref	90	88
	1	78	100
	2	92	100
	ref	8	100

Table S 9. Catalytic results using **1**, **2** or the reference catalyst ("ref") [NiBr₂(dppe)] for C(sp²)-C(sp³) couplings. Reactions were carried out with 10 mol% catalyst at room temperature for 20 h in toluene.

		Conversion [%]	Selectivity [%]
	1	65	75
	2	73	90
	ref	86	84
	1	70	93
	2	73	95
	ref	100	100

7. Computational details

All calculations were carried out using the ORCA 5.0.3 package in the gas phase.^{19,20} For all ORCA calculations, atom-pairwise dispersion corrections with the Becke-Johnson damping scheme (D3BJ) were utilised.^{21,22} Density fitting techniques, also called resolution-of-identity approximation (RI), were used for the GGA calculations.

Geometry optimisations and frequency analyses, to confirm the absence of any imaginary frequencies, were carried out at the TPSS^{23,24}/def2-TZVP^{25,26} level of theory. The geometry optimisations of **1** and **2** are based on the coordinates obtained from the crystal structure. Time-dependent density functional theory (TD-DFT)²⁷ calculations at the TPSS^{23,24}/def2-TZVP^{25,26} level of theory were utilised to investigate the underlying electronic transitions. For plotting the spectra, the orca_mapspc programme was used with a 2500 cm⁻¹ line broadening for the UV/Vis spectra. For the generation of the calculated IR spectra, also the orca_mapspc programme was used. For the plot of the difference densities the orca_plot programme was used.

Table S 10. Löwdin charges from Löwdin population analysis. Level of theory: TPSS, def2-TZVP. dppm = Methylenebis(diphenylphosphane)

	[NiBr ₂ (PSP)] (1)	[NiI ₂ (PSP)] (2)	[NiBr ₂ (dppm)]	[NiI ₂ (dppm)]
Ni	-0.939615	-0.990836	-1.045391	-0.998144
P	0.629128, 0.628393	0.641930, 0.643324	0.771001, 0.822381	0.765617, 0.814405
Hal	0.005878, 0.012959	0.025712, 0.048805	0.084350, 0.080942	0.073791, 0.076647

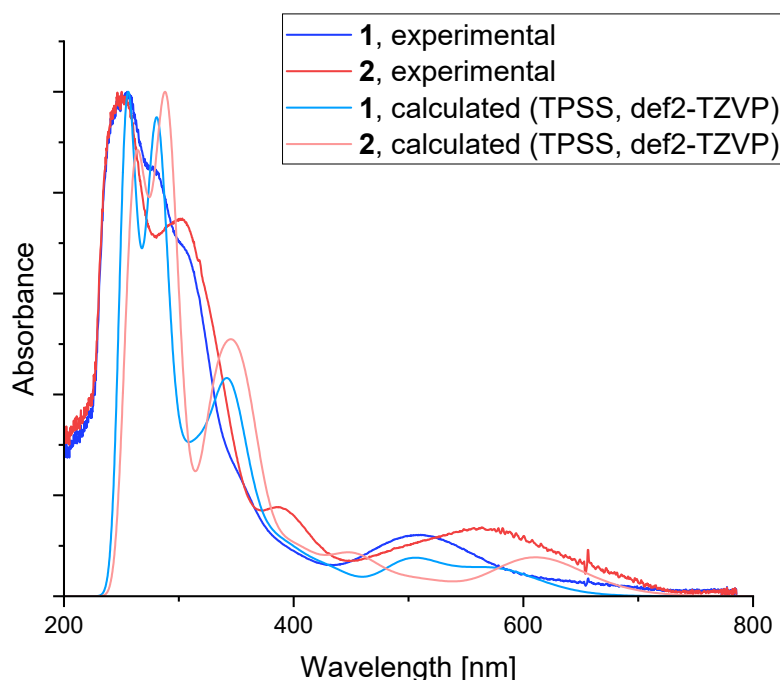


Figure S 31. TD-DFT calculated UV/Vis spectra of **1** and **2** (level of theory: TPSS, def2-TZV) together with the experimentally obtained spectra DCM solutions ($c = 1 \cdot 10^{-4} \text{ mol L}^{-1}$).

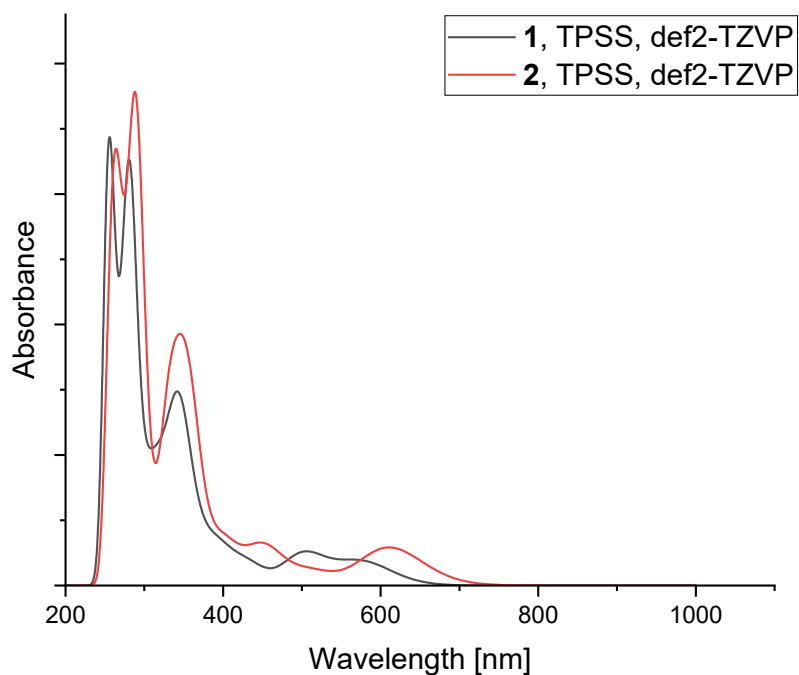


Figure S 32. TD-DFT calculated UV/Vis spectra of **1** and **2** (level of theory: TPSS, def2-TZVP).

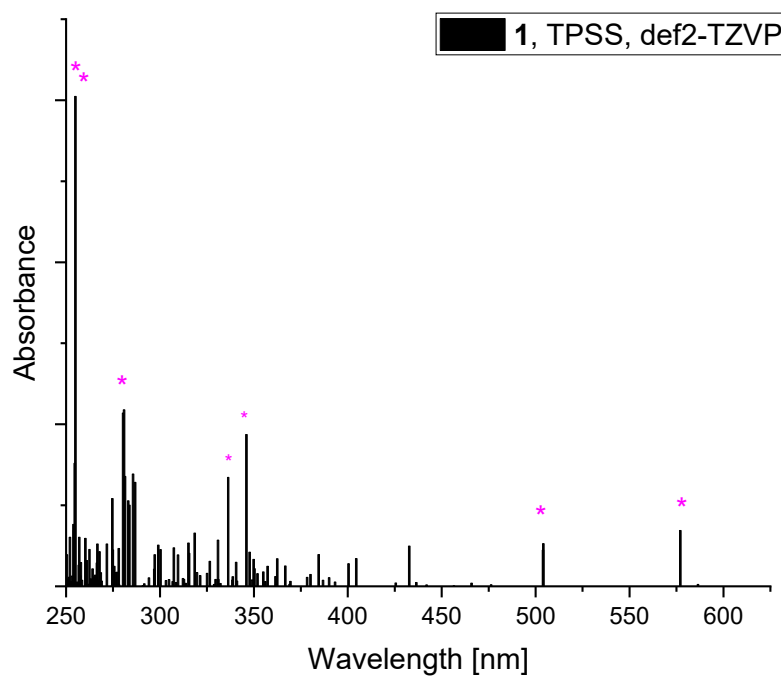


Figure S 33. TD-DFT calculated UV/Vis spectrum of **1** indicated by the respective oscillator strengths (level of theory: TPSS, def2-TZVP). Transitions with high oscillator strengths are highlighted and evaluated with respect to their difference density in Table S 10.

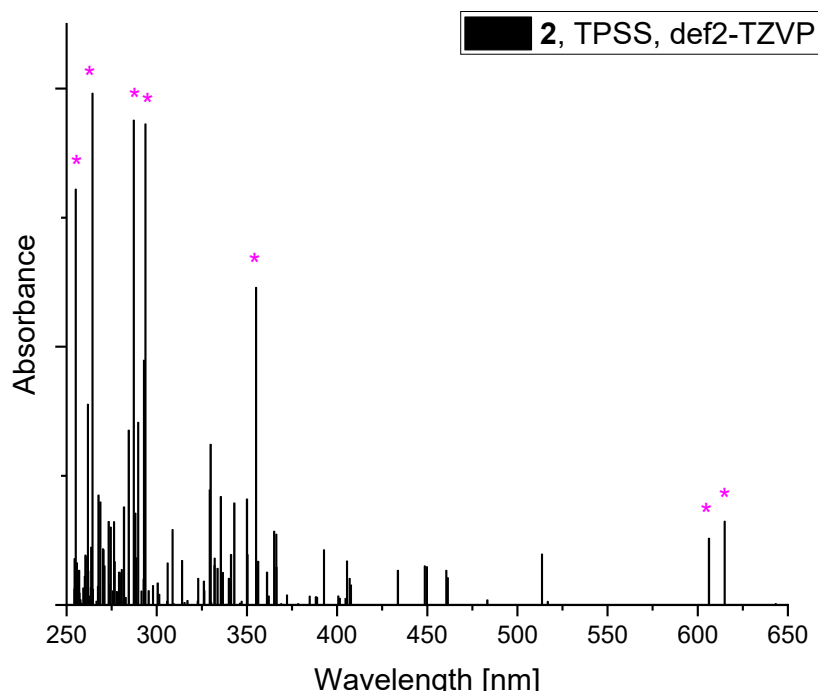


Figure S 34. TD-DFT calculated UV/Vis spectrum of **2** indicated by the respective oscillator strengths (level of theory: TPSS, def2-TZVP). Transitions with high oscillator strengths are highlighted and evaluated with respect to their difference density in Table S 11.

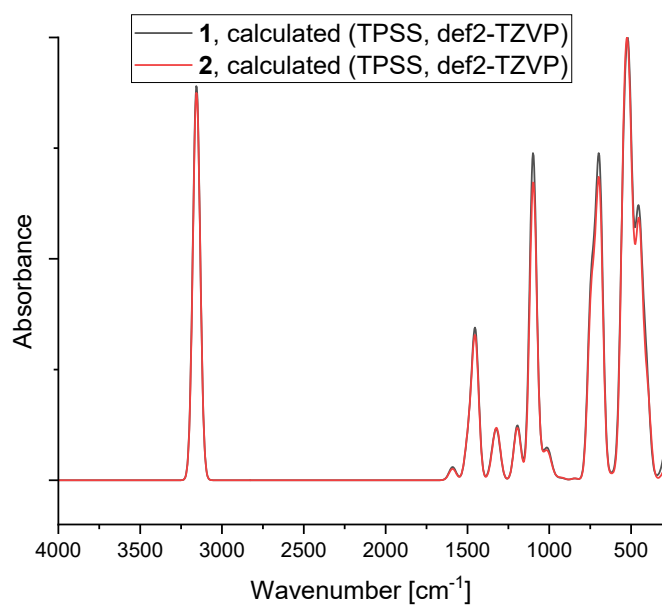


Figure S 35. Normalized calculated IR spectra of **1** and **2** (level of theory: TPSS, def2-TZVP).

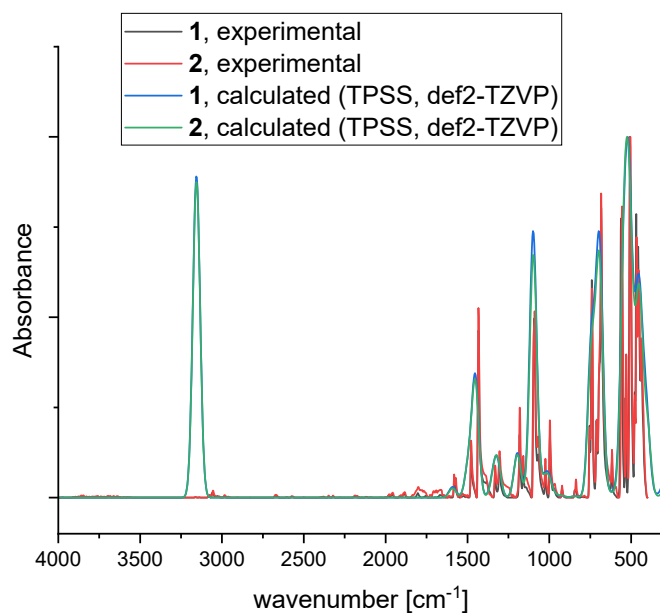


Figure S 36. Comparison of the normalized experimental and calculated IR spectra of 1 and 2 (level of theory: TPSS, def2-TZV). A systematic blueshift of the frequencies is observed.

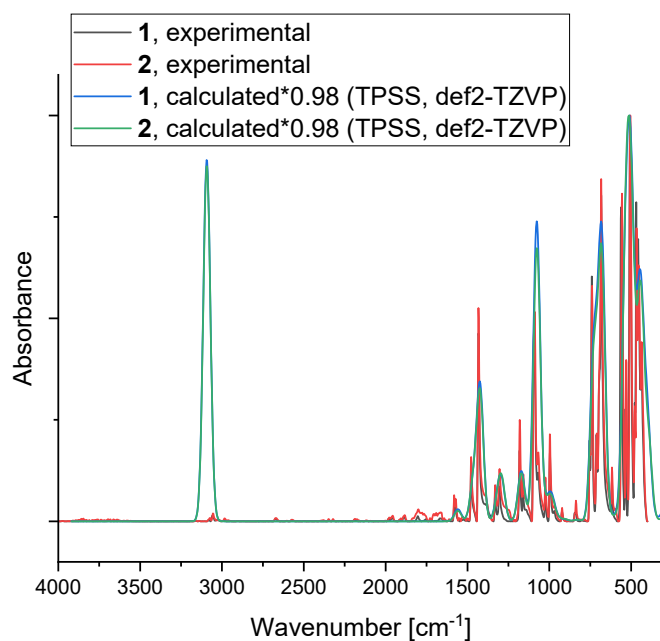


Figure S 37. Comparison of the normalized experimental and calculated IR spectra of 1 and 2 (level of theory: TPSS, def2-TZV). To counterbalance the commonly observed blue-shift of DFT functionals, the obtained energies were scaled using a scaling factor of 0.98. This scaling factor aligns very well with reported scaling factors for the DFT calculation of ground state harmonic vibrational frequencies.²⁸

Table S 11. Difference densities obtained for **1** from TD-DFT calculations, including the calculated wavelengths and oscillator strengths of the respective transitions. Transitions proceed from blue to red. Level of theory: TPPS, def2-TZVP, surface iso values = ± 0.001 .

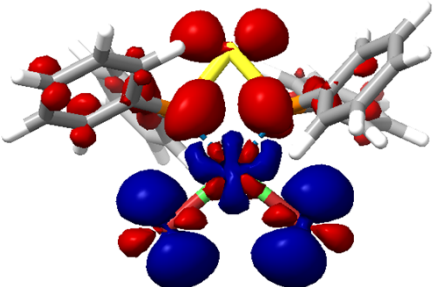
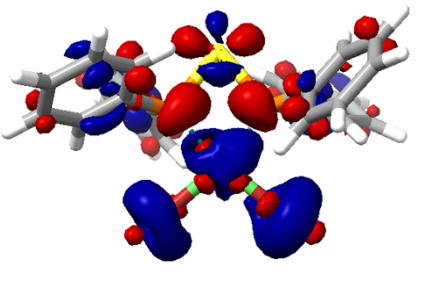
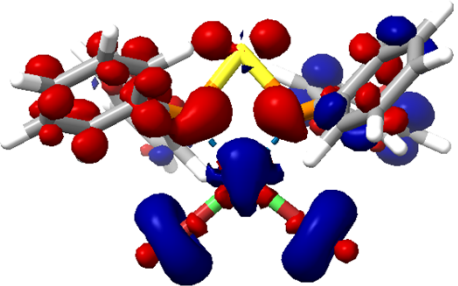
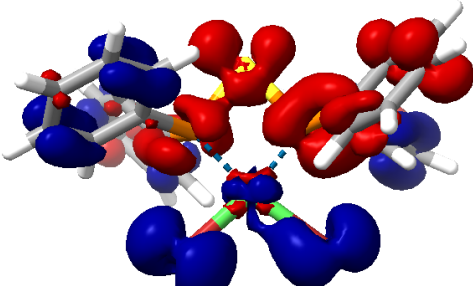
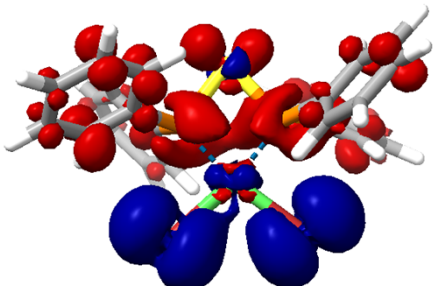
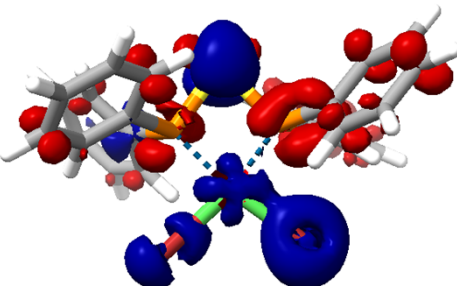
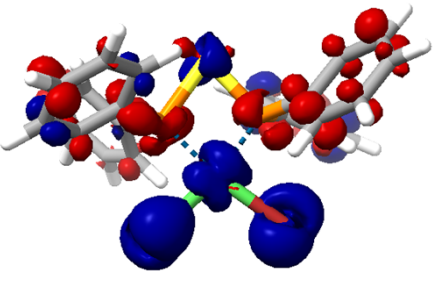
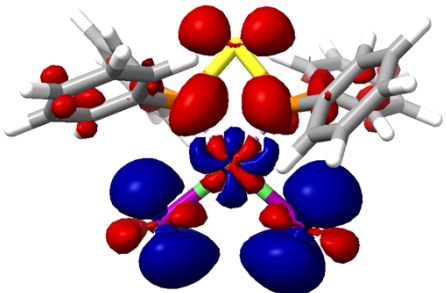
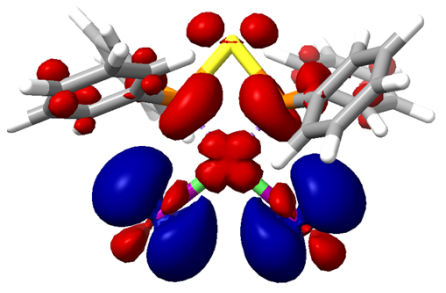
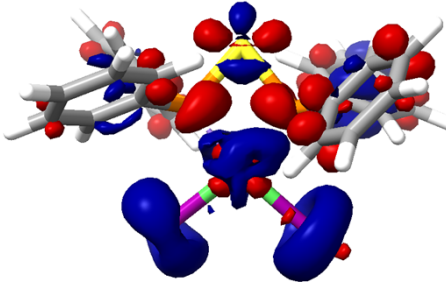
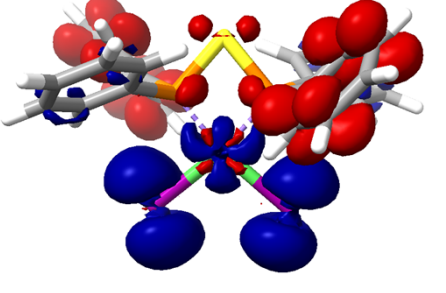
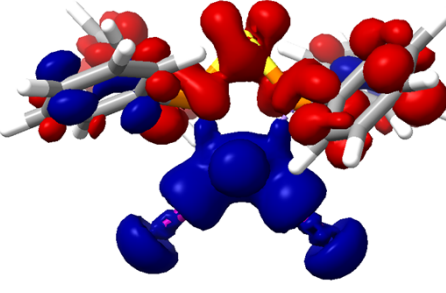
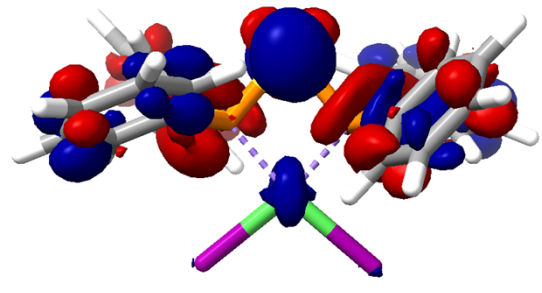
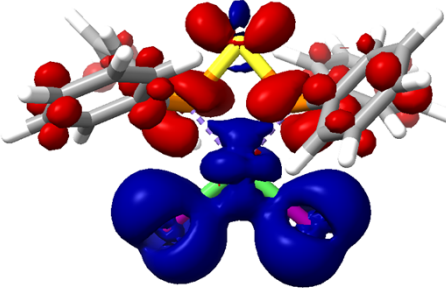
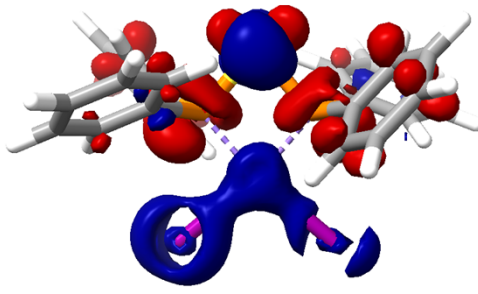
 <p>Transition 2 577 nm, 0.015880425 HOMO-1 (73% Ni, 15 % Br) \rightarrow LUMO (38% Ni, 20% P and S, 14 % Br)</p>	 <p>Transition 33 346 nm, 0.043180516</p>
 <p>Transition 38 336 nm, 0.031001622</p>	 <p>Transition 72 281 nm, 0.031247648</p>
 <p>Transition 73 281 nm, 0.050212312</p>	 <p>Transition 104 255 nm, 0.139345570</p>
 <p>Transition 105 254 nm, 0.035033091</p>	

Table S 12. Difference densities obtained for **2** from TD-DFT calculations, including the calculated wavelengths and oscillator strengths of the respective transitions. Transitions proceed from blue to red. Level of theory: TPPS, def2-TZVP, surface iso values = ± 0.001 .

 <p>Transition 2 615 nm, 0.014931428 HOMO-2 (80% Ni, 7% I) \rightarrow LUMO (35% Ni, 17% P and S, 18% I)</p>	 <p>Transition 3 606 nm, 0.011868699 HOMO-1 (80% I) \rightarrow LUMO (35% Ni, 17% P and S, 18% I)</p>
 <p>Transition 35 355 nm, 0.056656899</p>	 <p>Transition 39 346 nm, 0.000285545</p>
 <p>Transition 69 293 nm, 0.085849947</p>	 <p>Transition 76 287 nm, 0.086533368</p>
 <p>Transition 101 264 nm, 0.091335981</p>	 <p>Transition 118 225 nm, 0.074201486</p>

8. References

1. Stoe&Cie, *Journal*, 2005, X-RED, Program for data reduction and absorption correction, X-RED, Program for data reduction and absorption correction.
2. G. M. Sheldrick, *Acta. Cryst. A*, 2015, **71**, 3-8.
3. G. M. Sheldrick, *Acta. Cryst. B*, 2015, **71**, 3-8.
4. L. J. Farrugia, *J. Appl. Crystallogr.*, 2012, **45**, 849-854.
5. K. Brandenburg and M. Berndt, *Journal*, 1999, Diamond - Crystal and Molecular Structure Visualization.
6. C. J. Ballhausen and A. D. Liehr, *J. Am. Chem. Soc.*, 1959, **81**, 538-542.
7. O. A. Qamar, C. Cong and H. Ma, *Dalton Trans.*, 2020, **49**, 17106-17114.
8. M. C. Browning, J. R. Mellor, D. J. Morgan, S. A. J. Pratt, L. E. Sutton and L. M. Venanzi, *J. Chem. Soc.*, 1962, 693-703.
9. W. Kläui, K. Schmidt, A. Bockmann, P. Hofmann, H. R. Schmidt and P. Stauffert, *J. Organomet. Chem.*, 1985, **286**, 407-418.
10. A. Okuniewski, D. Rosiak, J. Chojnacki and B. Becker, *Polyhedron*, 2015, **90**, 47-57.
11. F. A. Cotton, L. R. Falvello, M. Tomas, G. M. Gray and C. S. Krainhanzel, *Inorg. Chim. Acta*, 1984, **82**, 129-139.
12. P. E. Sues, A. J. Lough and R. H. Morris, *Chem. Commun.*, 2014, **50**, 4707-4710.
13. H.-K. Fun, S. Chantrapromma, I. A. Razak, Q.-F. Zhang and X.-Q. Xin, *Acta. Cryst. E*, 2001, **57**, m190-m191.
14. W. Kläui, W. Eberspach and R. Schwarz, *J. Organomet. Chem.*, 1983, **252**, 347-357.
15. P. Porta, A. Sgamellotti and N. Vinciguerra, *Inorg. Chem.*, 1968, **7**, 2625-2629.
16. P. Porta, A. Sgamellotti and N. Vinciguerra, *Inorg. Chem.*, 1971, **10**, 541-547.
17. J. M. Coleman and L. F. Dahl, *J. Am. Chem. Soc.*, 1967, **89**, 542-552.
18. S. Ataie and R. T. Baker, *Inorg. Chem.*, 2022, **61**, 19998-20007.
19. F. Neese, *WIREs Comput. Mol. Sci.*, 2017, **8**, e1327.
20. F. Neese, *WIREs Comput. Mol. Sci.*, 2011, **2**, 73-78.
21. S. Grimme, J. Antony, S. Ehrlich and H. Krieg, *J. Phys. Chem.*, 2010, **132**, 154104.
22. S. Grimme, S. Ehrlich and L. Goerigk, *J. Comp. Chem.*, 2011, **32**, 1456-1465.
23. V. N. Staroverov, G. E. Scuseria, J. Tao and J. P. Perdew, *J. Phys. Chem.*, 2004, **121**, 11507.
24. J. Tao, J. P. Perdew, V. N. Staroverov and G. E. Scuseria, *Phys. Rev. Lett.*, 2003, **91**, 146401-146404.
25. F. Weigend, *Phys. Chem. Chem. Phys.*, 2006, **8**, 1057-1065.
26. F. Weigend and R. Ahlrichs, *Phys. Chem. Chem. Phys.*, 2005, **7**, 3297-3305.
27. C. Adamo and D. Jacquemin, *Chem. Soc. Rev.*, 2013, **42**, 845-856.
28. D. O. Kashinski, G. M. Chase, R. G. Nelson, O. E. Di Nallo, A. N. Scales, D. L. VanderLey, E. F. C. Byrd, *J. Phys. Chem. A*, 2017, **121**, 11, 2265-2273.